Techniques of optical imaging in the presence of scattering

A thesis submitted for the degree of
Doctor of Philosophy
to
Jawaharlal Nehru University

by

Bapan Debnath

Raman Research Institute
C. V. Raman Avenue
Bangalore - 560080

June 21, 2024

Declaration

I, **Bapan Debnath** (Enrolment No.: RRI/2016/005), declare that the work reported in this thesis titled ***Techniques of optical imaging in the presence of scattering***, is entirely original. This thesis is composed independently by me at **Raman Research Institute** under the supervision of **Prof. Hema Ramachandran** (Deceased) and **Prof. Reji Philip**. It is the result of my work unless otherwise stated. I further declare that the subject matter presented in this thesis has not previously formed the basis for awarding any degree, diploma, membership, associateship, fellowship, or other similar titles of any university or institution. I also declare this thesis has been checked through the plagiarism software DrillBit.

Signature of the Supervisor	Signature of the Candidate
Prof. Reji Philip	**Bapan Debnath**

Certificate

This is to certify that the work contained in the thesis titled ***Techniques of optical imaging in the presence of scattering***, submitted by **Bapan Debnath** (Enrolment No.: RRI/2016/005) to the Jawaharlal Nehru University for the award of the degree of **Doctor of Philosophy (Ph.D.)** in Physical Sciences, is his original research work carried out between July, 2016 - June, 2024, at Raman Research Institute, Bengaluru, India. The results embodied in the thesis have not been submitted to any other University or Institute for the award of any degree or diploma.

Signature of the Director	Signature of the Supervisor
Prof. Tarun Souradeep	**Prof. Reji Philip**

Acknowledgement

Writing an acknowledgement is the toughest part in a thesis. Properly acknowledging all the persons is very critical and challenging, may be because we need to give proper credit each and everyone who contributed to my life directly or indirectly. Also, while writing this there is always a mental fight going on between logic and emotions, and you start to wander what to write so that nobody gets offended. Sometime you think, let just state something like, "Thank you UNIVERSE," other times you would prefer, let just acknowledge only the Supervisor, and collaborators, but ultimately I ended up in a state where I thought to write a long acknowledgement mentioning the people who even were like a tangent in my circular life. That would have been a perfect and best acknowledgement, isn't it? But alas that's just... impossible to write. Hence, I would state 'whatever' comes to my mind. So, 'without a further delay, let's get started.'

First and foremost, I would like to thank and convey my sincere gratitude to my former supervisor Prof. Hema Ramachandran for her supervision, immense support, inspiring discussions, and for providing a state of the art facilities in the lab. She always understood the problem/question I am facing/posing in all the discussions. She constantly motivated me to think in a different way. I am grateful to provide me the opportunity to join her lab and working with her.

Secondly, I would like to thank my supervisor Prof. Reji Philip for his supervision, encouraging discussions, and for providing a state of the art facilities in the lab. His support has always uplifted me during the difficult time, and kept me going. In all the discussions, he always tried to understand the problem, even though this was a new field to him. I thank him

to believed in me and to provide the support in the stressful time..

I would like to thank our collaborators Dr. Jayashree A. Dharmadhikari, Dr. Aditya K. Dharmadhikari for their support, encouraging discussions. They have been excellent collaborators from the start.

Further, I would like to thank our collaborators Prof. Fabien Bretenaker, Prof. Mehdi Alouini, Prof. Julien Fade for fruitful discussions and encouragement.

I would like to thank Prof. Shankar Dhar and Prof. Rupamanjari Ghosh from Shiv Nadar University, Greater Noida, Uttar Pradesh, to allow us to do the fog experiment at the campus premises and to provide the hospitality. I would also like to thank Prof. R. Srikanth from Poornaprajna Institute of Scientific Research, Bengaluru, Karnataka, to perform the rest of the experiment at their and also to provide the hospitality.

I would like to thank Dr. Saptarishi Chaudhuri for discussions and his support. He always encouraged me to solve a problem in a very simple way. Various discussions with him about the experiment made a problem more easier to solve.

Also, I would like to thank Meena M. S. for collaborating in developing and characterizing various electronic components and equipment for the experiments. Several discussions with her about the electrical and electronic components made me stronger in these fields and also made me confident to handle complex electronics component.

I would like to thank Dr. Saptarishi Chaudhuri and Prof. Andal Narayanan for being part of my thesis advisory committee. Their appropriate comments and fruitful suggestions in the annual reviews helped me keep my research on track.

I would like to thank my colleague Shashank Kumar to work with me on the fog experiment and also for the productive discussions with him.

I would like to thank the members of the workshop, library, administration, accounts, store, and carpentry for their support throughout my stay, especially Ibrahim from the workshop. I sincerely thanks Savitha, Shiva, and Manjunath for their help. I would also like to thank the canteen staff for providing healthy food, gardeners for making the campus beautiful and alive, cleaning staff for making the campus and hostel clean, and security staff, shuttle drivers,

electricians, and clinic staff for their respective work. I would like to thank G. B. Suresh and Muneeswaran for their help. I would like to thank Jacob Rajan and the whole computer section department for their help. I sincerely acknowledge the effort paid by Mangla Ji and her team at Vyalikaval hostel for serving us hygienic foods as per our demand and taking care of every student in a very homely manner. I would like to thank institute sport's committee members for running the sports smoothly, and providing an pleasant ambiance where irrespective of the sports skills everyone is welcomed to join any sport.

I would also like to thank Surya Narayan Sahoo for the productive scientific, technical, non-technical and political discussions which helped me not only to understand a related scientific topic to my PhD work, but also about completely unrelated topic like how the economics of the world could be better.

I would like to thank my lab mates Reshma, Shovan, Silpa, Snehal, Sukanya for the journey we shared in the lab.

I would like to thank my batch mates Anand, Pradosh, Rishab and Sanchari.

I am indebted to my friends, seniors, and juniors with whom I shared this journey. I wholeheartedly thank Maheswar Da, Rishab, Avik, Subhajit Da, Tanuman, Agnibha, Shovan, Dipak, Sanchari, Abhishek, Sagar Da, Kaushik Da, Anindya Da, Sandeep, Souradeep Da, Sourav Da, Ankita Di, Animesh Da, Pampa Di for this journey, and I will never forget the exciting life I spent together with them.

I would like to thank all the members of the football committee. All of them, even if someone came only once so that one day we don't even have 6 people (minimum of people to at least start), but the next day we have 16.

I truly acknowledge my friends Saikat, Ranita, Vishnu, Ashish, Rajkumar, Ion, Arup Da, Rajkumar Da, Arun, Nishant, Subodh, Vardhan, Arsalan, Adwaith, Sebanti, Anirban, Swarnak, Irla, Saichand, Subhadip Da.

I would also like to thank my juniors Soumen, Sayantan, Jasim, Sovan, Gourab, Sayari, Rupak, Srijit, Swarnava, Anirban (Mishra), Sachi, Saumya, Abhishek (Gadai), Anson, Punit.

I would also like to thank the anonymous referees who helped me, in many ways, under-

stand our work more clearly.

I sincerely apologize if I miss someone whom I should have acknowledged.

I would like to thank my tution teacher in B. Sc., Dr. Jyotirmoy Guha, a professor in Santipur college, West Bengal, who not only taught us the topics in the curriculum, but also told exciting day to day research as a fantastic story. I loved the way he always understood the students' question first, and then only gave an answer. If the student is not understanding, he will take some time to think the student's perspective, and then only he reattempted to answer. Also, just because he doesn't know the answer, he never replied with a jargon, given a false statement, ignored the question or disrespected the student. Also, I admired his calm personality.

The last part of an acknowledgement is even more harder, where everyone tries to express their family's contribution to their lives since it's, actually, very very difficult. I am here it's because of my family - my mother (Gita Debnath), my father (Bhanu Debnath), and my brother (Tarak Debnath). They never doubted me even for a second. They gave me complete freedom to choose my career. 'I love you all'. Also, I want to mention my cousin Kalyan, with whom I shared my life journey starting from our childhood. Also, I want to mention my beloved wife Sreya for her unwavering support. I dedicate this thesis to my family.

পরিবারকে উৎসর্গ

Contents

Synopsis

Scattering is ubiquitous; everything we see is because of the scattering of light. However, if the medium through which light passes is turbid, it gives rise to deleterious effects like reduced visibility resulting in the inability to see or image an object. This effect arises due to the optical inhomogeneities, which lead to an altering of the direction of propagation and polarization of light. The ballistic photons that travel in a straight line retain properties such as polarization, modulation frequency, and phase, and are responsible for imaging. These photons must be extracted from the vast amount of diffusive photons to image the object.

This thesis reports investigations to develop techniques of imaging through various turbid media, e.g., fog, smoke, milk in water solution, etc. We have used a technique, namely the quadrature lock-in discrimination (QLD) algorithm, to make it simple and straightforward. The thesis is structured in the manner described below:

Chapter 1 gives a brief introduction to the scattering of light in turbid media, the behavior of photons in these media, and imaging using different types of photons.

Chapter 2 describes a detailed theory with the mathematics of the technique, QLD, along with the simulation, code, and simulated results.

Chapter 3 reports a field application of imaging in which we image through fog. In this experiment, we image a modulated LED, as in beacons, at a distance of 150 m, in which the visibility was merely 50 m. This experiment also makes it possible to discriminate between the modulated light source and any nearby sources of light that can dazzle the viewer.

Chapter 4 presents an enhancement of the contrast of the images obtained through fire and smoke. A blue LED and a blue filter are used in this technique. Fire is simulated using

candle flame, and smoke is produced by a smoldering incense cone kept inside a chamber. The modulated light from the source travels through the flame and smoke, is reflected by the object, passes through the medium again, and is finally captured by a camera. After applying the QLD technique, we observe a significant improvement in the image contrast of the object.

Chapter 5 demonstrates a proof-of-principle imaging technique using an acousto-optic modulator (AOM). In this experiment, the demodulation of the QLD technique is done on an AOM as opposed to using the software. Using a series of frames, we saw an enhancement in the image contrast. We also performed systematic imaging by varying the turbidity of the medium and camera parameters such as exposure time, frame rate, and the total number of frames to investigate its effect on the improvement of the image contrast.

Chapter 6 summarizes the essential observations and conclusions drawn from the experiments reported in this thesis, followed by the future scope of the work.

List of Publications

1. Imaging through fog using quadrature lock-in discrimination

   Shashank Kumar, **Bapan Debnath**, Meena M. S., Julien Fade, Sankar Dhar, Mehdi Alouini, Fabien Bretenaker, Hema Ramachandran

   OSA Continuum, **4**, 1649 (2021)

   arXiv:2105.08524

2. Improved imaging through flame and smoke using blue LED and quadrature lock-in discrimination algorithm

   Bapan Debnath, Jayashree A. Dharmadhikari, Meena M. S., Hema Ramachandran, Aditya K Dharmadhikari

   Optics and Lasers in Engineering, **154**, 107045 (2022)

3. Imaging through scattering media using an acousto-optic modulator

   Bapan Debnath, Meena M. S., Jayashree A. Dharmadhikari, Saptarishi Chaudhuri, Reji Philip, Hema Ramachandran

   Applied Optics, **62**, 6609 (2023)

List of Figures

Chapter 1

Introduction

Fig. 1.1. A photograph of the main (administrative) building and the lawn of Raman Research Institute along with blue sky and white cloud. Image courtesy: Self.

In our childhood, at least once, we have all pondered the cause of the magnificent phenomenon, "The Blue Sky". The reason is also as stunning as the phenomenon known as scattering. We also observe some delightful events in our daily lives due to scattering, e.g., the red color of sunset, the white/black color of clouds, etc. Scattering is a ubiquitous phenomenon. The whole electromagnetic spectrum, including the 'visible light' spectrum, is scattered incessantly. Scattering is the reason we perceive the world through our eyes. Every

color we see is because of scattering. To show a glimpse of the two scattering phenomena "the blue sky", and the white color of clouds, and also to commemorate our beautiful institute, a photograph of the main (administrative) building and the lawn of Raman Research Institute along with the blue sky and white cloud is shown in Fig. 1.1. Let's first review two basic topics, optical media and turbid media.

1.1 Optical media

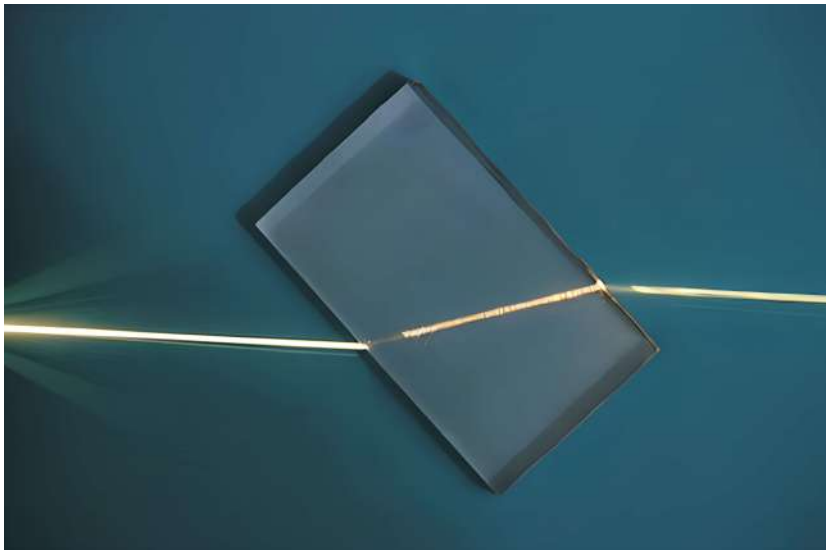

Fig. 1.2. Example of an optical medium: Glass slab. Image courtesy: Wikipedia.

In general, a material through which light propagates is referred to as an optical medium. Although no medium permits the whole electromagnetic spectra to propagate through, it depends on the properties of the medium which part of the spectrum can transmit. E.g., visible light (400 - 700 nm) may pass through water without being much reflected or absorbed, but anything below 200 nm and above 1µm shows a significant to strong absorption. If a medium transmits a significant amount of light, such a medium is called transparent medium. Glass has a transmission window at optical spectrum, hence glass is transparent to visible light. An example of an optical phenomenon, refraction, along with the optical medium, glass, is shown in Fig. 1.2.

1.2 Turbid media

If a medium randomly scatters or diffuses the light in any direction, is referred to as a scattering medium or turbid medium. This can happen because of the medium constituents, small particles such as dust, smoke, or even atoms, molecules etc. Although turbid media are often translucent, meaning that light cannot pass through it without scattering, it can nonetheless allow some light to pass through without any interaction with the medium.

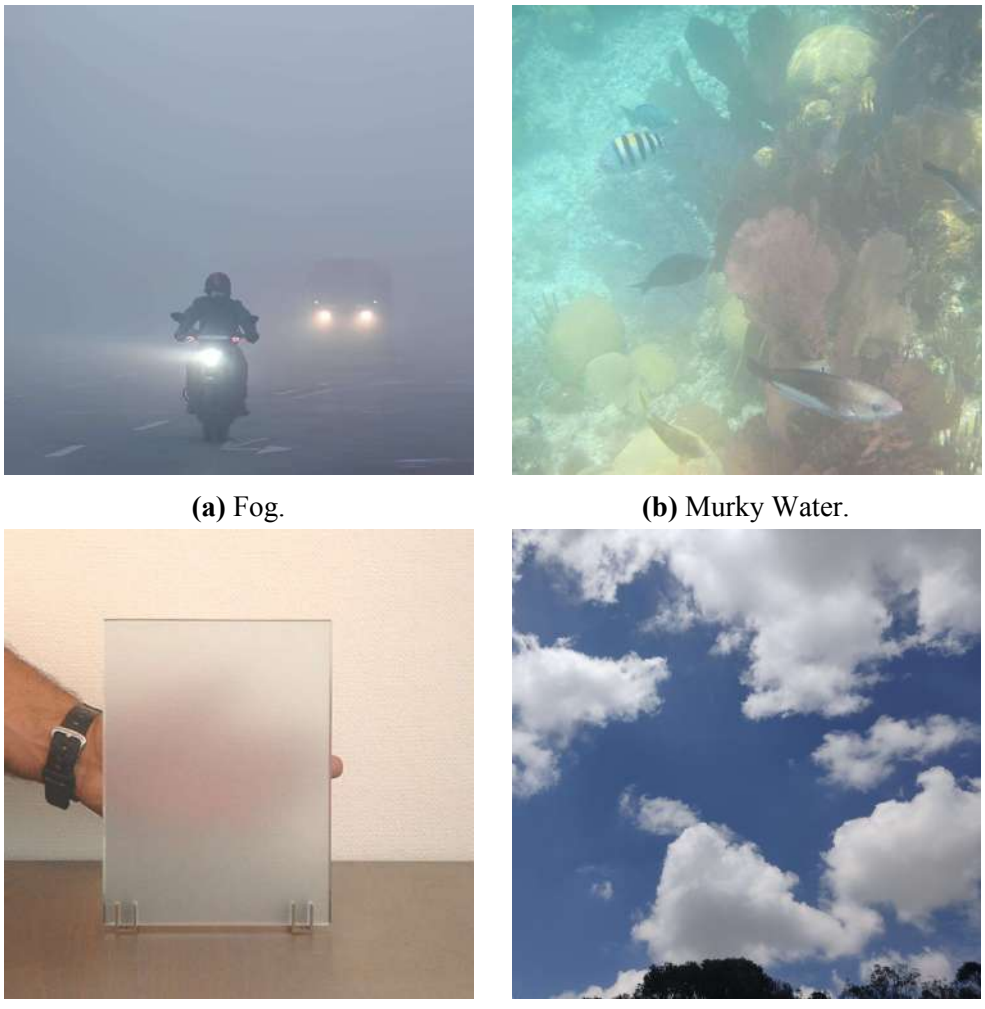

(a) Fog. **(b)** Murky Water.

(c) Diffused Glass. **(d)** Cloud.

Fig. 1.3. Turbid Media. Image Courtesies: (a) Hindustan Times, (b) Tropical Snorkeling, (c) Stack Exchange, (d) Self.

Turbid media can be found in the atmosphere, e.g., fog, cloud, smoke, haze, smog, etc. Liquid substances like milk, muddy water, etc., are also examples of such media. Diffused

glass, used in windows or doors to obscure direct light but to pass dispersed light, is a turbid medium. Biological tissues are one type of scattering media in which the light undergoes a large amount of random scattering. A few turbid media are shown in Fig. 1.3.

Although, because of scattering, we see wonderful phenomena, it has several significant implications. For example, it makes objects challenging to see that are hidden behind a scattering medium. The light coming from an object is randomly scattered by the medium in all directions, obscuring the object. Here, we should remember that, along with scattering, there will be absorption in the medium.

1.3 Scattering

When light passes through turbid media, it follows a zigzag path because of the random scattering of the photons caused by the suspended particles. The characteristics of scattering depend on the shape, size, and concentration of the scatterers, as well as the wavelength of the light. The dependence of the scattering on the relative size of the particle with respect to the wavelength of the light is parameterized using a term called size parameter, defined as $x = 2\pi r/\lambda$, where r is the radius of the scatterer, and λ is the wavelength of the light. Scattering is categorized into three classes depending on the x values. The first and foremost is Rayleigh scattering. This type of scattering happens if the size parameter is less than unity ($x << 1$) or the radius (r) of the scatterer is at least one order lower in magnitude than the wavelength (λ) of the light. The amount of scattering is inversely proportional to the fourth power of the wavelength of the light, i.e., the larger the wavelength, the less light is scattered. Also, the scattering intensity is proportional to the 6th power of the radius of the scatterer and the square of the cosine of the scattering angle. In Fig. 1.4, we can see a reddening or yellowish of the sky nearest to the sun and bluing of the sky furthest away from the sun. It is because the red-yellow part of the spectrum is less scattered, and directly reach our eyes, conversely, the blue part of the spectrum is scattered more and reach our eyes through multiple scattering. Even though violet colour is scattered more compared to the blue wavelength, our

Fig. 1.4. The alteration in the color of the sky at sunset. Red color nearest to the sun, blue furthest away along with gray/white cloud. Image courtesy: Wikipedia.

eyes are more sensitive to blue than violet making the sky blue. The scattering is symmetric in the forward and reverse direction in this regime, but an increase in the size parameter leads to an asymmetric distribution. It is larger in the forward direction than in the reverse direction. This phenomenon happens for $x \simeq 1$, and the scattering is called as Mie scattering. In this regime, the amount of scattering is roughly independent of the wavelength of the light. Since, the size of the water particle in clouds is comparable to the wavelength of the light in the visible spectrum, all the color is scattered in a same amount, leading to the white colour of the cloud. It should be mentioned that depending on the water particle size and distance, and angle of the sunlight, clouds might appear black because of the absorption of the light by water droplets. In this case, the scattering intensity depends on the size of the scatterer in a very complex way. The actual dependency is via infinite series of special functions. The

white/gray colour of the clouds in Fig. 1.4 is caused by Mie Scattering. If the wavelength of the incident light is constant, the greater the particle size, the more scattering happens in the forward direction. Lastly, for $x >> 1$, the objects act as geometric shapes, leading to Geometric Optics phenomena.

The scattering of light also depends on the coherence properties of the source. If the light is coherent, a situation occurs in which there is an enhancement of the backscattering of the light. This phenomenon is called coherent backscattering.

Scattering is also categorized into (i) Elastic scattering, in which the internal structure of the particle doesn't change. Therefore the energy of the incident photon remains the same before and after the scattering, only its direction changes. Since there is no energy transfer, the particle number is also stays constant. One famous example of this type of scattering is Rutherford scattering experiment. Other examples are Thomson scattering, Rayleigh and Mie scattering. (ii) Inelastic scattering, in which the internal structure of the particle changes, leading to a change in energy of the incident photon. In this case, the particle number might not stays constant. One example of this type of scattering is Compton scattering. Scattering is also categorized into classes depending on the energy of the photons, such as Compton scattering, Raman scattering, Brillouin scattering etc.

1.4 Behaviour of light passing through turbid media

When light passes through a turbid media, most of the photons are either scattered or absorbed. However, a few photons travel through the medium in a relatively straight line with minimum deviation. These are referred to as ballistic photons [1]. They retain the properties such as the direction of propagation, polarization, and phase of the incident light, and because of this, these photons have the image producing capability. However, the ballistic photon number decreases rapidly with an exponential dependence with an increase in propagation distance. Photons that are near forward scattered and whose path is not far from ballistic photons are called snake photons because they follow a snake-like pattern as they travel

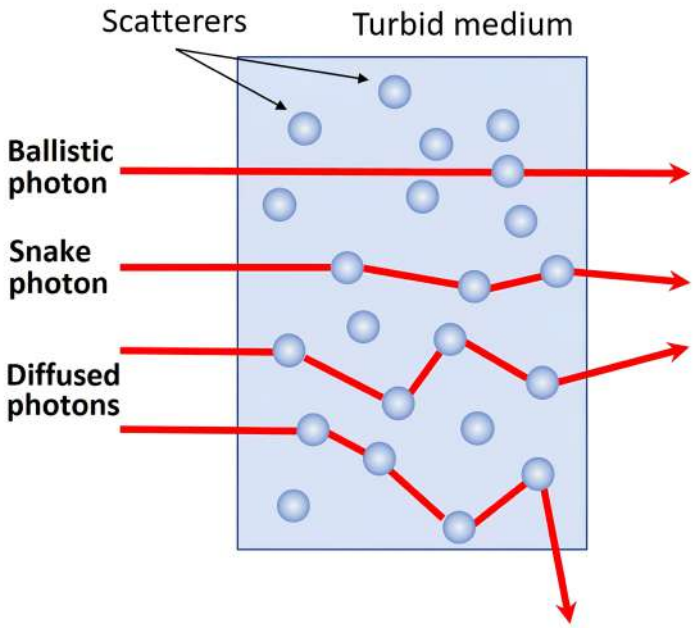

Fig. 1.5. Trajectory of Ballistic, Snake, and Diffused photons. The image is taken from Ref. [2].

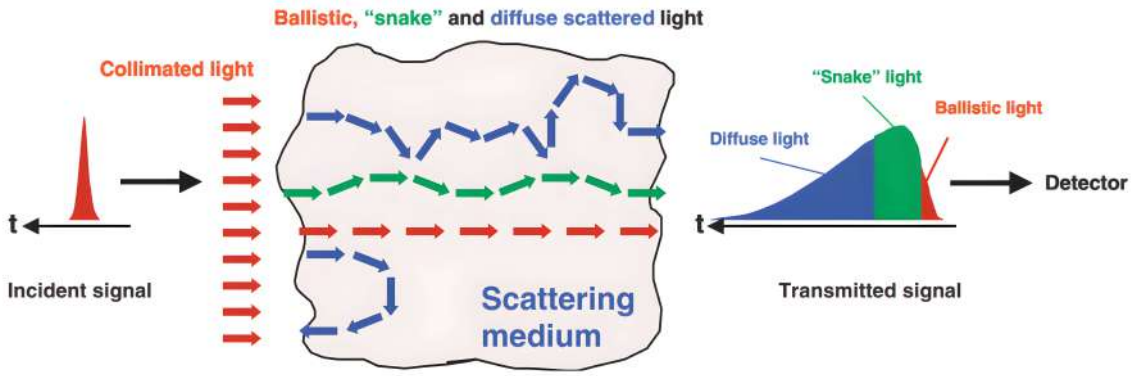

Fig. 1.6. Trajectory of Ballistic, Snake, and Diffused photons. The image is taken from Ref. [3].

through a medium. Lastly, there are photons that are multiply scattered in random angles over all directions, such that the paths are scrambled, and the original direction is lost. These are referred to as diffused photons. Diffused photons will overwhelm the number of ballistic photons for a significant scattering depth, making the detector capturing the light, saturated. Consequently, the image will also be hazy and obscure or may be completely noisy. The

trajectories of these three kinds of photons are shown in Fig. 1.5. It is immediately apparent that the ballistic photons reach the other side of the scattering medium earliest, followed by snake photons, and lastly diffused photons after interacting with the medium multiple times. The temporal point spread function of this transmitted photon distribution is shown in Fig. 1.6.

1.5 Different types of imaging techniques

Since different types of photons show different characteristics, they can be studied to evaluate detailed properties about the medium, the source or any object that is hidden behind the scattering medium or embedded in it.

1.5.1 Imaging using diffused photons

If the amount of ballistic photons is very less compared to that of diffused photons that it is not measurable by a detector or the ballistic signal is below the shot-noise limit, the images of any object can still be formed by using the diffused photons. In this case one can still use the earliest arriving photons after propagating through the scattering medium to form the image of the object, since these photon still retain a small amount of image-bearing capabilities of the source. This can be performed by using time-gated photon counting devices or using a streak camera [4]. One cannot use this technique if all the photons are diffused. In this case one has to use some photon transport model to extract information of the object inside the scattering medium. Monte Carlo techniques can be used to accurately simulate the light propagation in turbid media. One can also use the diffusion approximation of the radiative transfer equation to model the same [5]. Another technique based on the memory effect uses speckle pattern of the medium. These techniques utilize iterative operations, Richardson-Lucy deconvolution algorithm [6, 7] to restore the undegraded image. These techniques mostly need a-priori information of the medium as a speckle pattern (point spread function) of the turbid medium. The experimental setup of a recent work [8] is shown in Fig. 1.7.

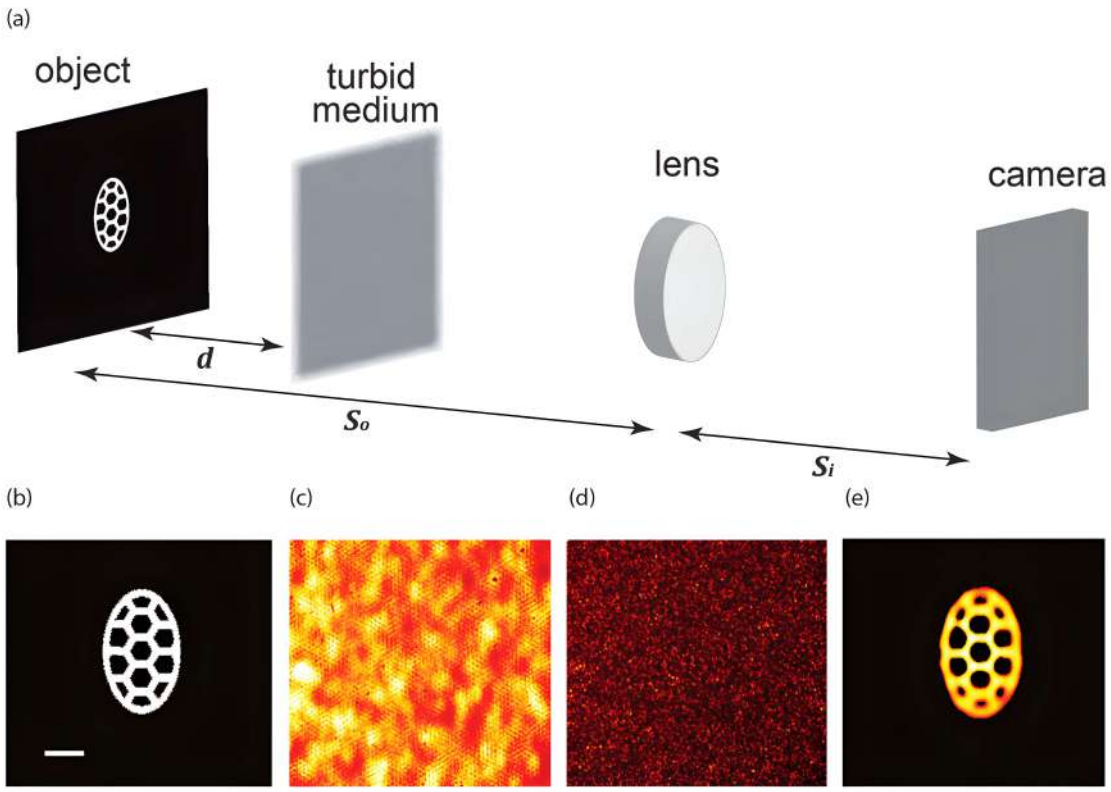

Fig. 1.7. Setup of a imaging experiment using memory-effect based deconvolution algorithm. (a) Experimental setup, (b) Image of the object without the turbid medium. Scale bar = 200 µm. (c) Image of the object with the scattering medium. (d) Speckle pattern of the setup. (e) Reconstructed image. The image is taken from Ref. [8].

1.5.2 Imaging using ballistic photons

The imaging can also be done by extracting the minute amount of ballistic and snake photons from the exceedingly large amount of diffused photons. The straightforward technique is to use a simple collimating grid as shown in Fig. 1.8. In this case the photons that are propagating parallel to the incident direction is transmitted along with a very few diffused photons.

An alternative approach to the collimating grid is by using spatial filtering at the Fourier plane [9] as shown in Fig. 1.9. This will increase the amount of ballistic photons to diffused photons, leading to an increase in signal-to-noise ratio (SNR), but at the cost of spatial resolution of the image.

In place of whole-field technique, scanning confocal imaging [10] system is also used to

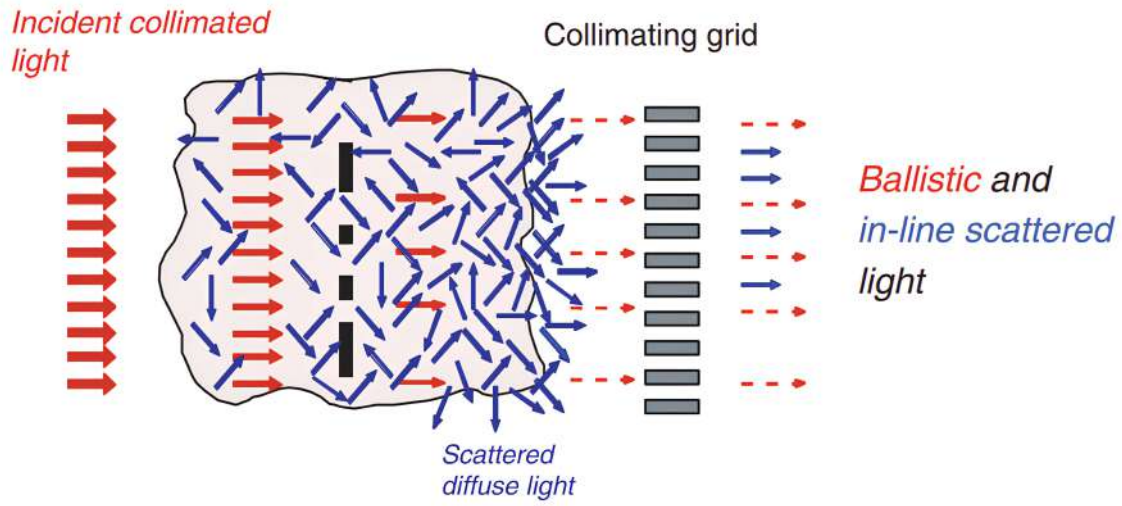

Fig. 1.8. Spatial filtering by collimating grid. The image is taken from Ref. [3].

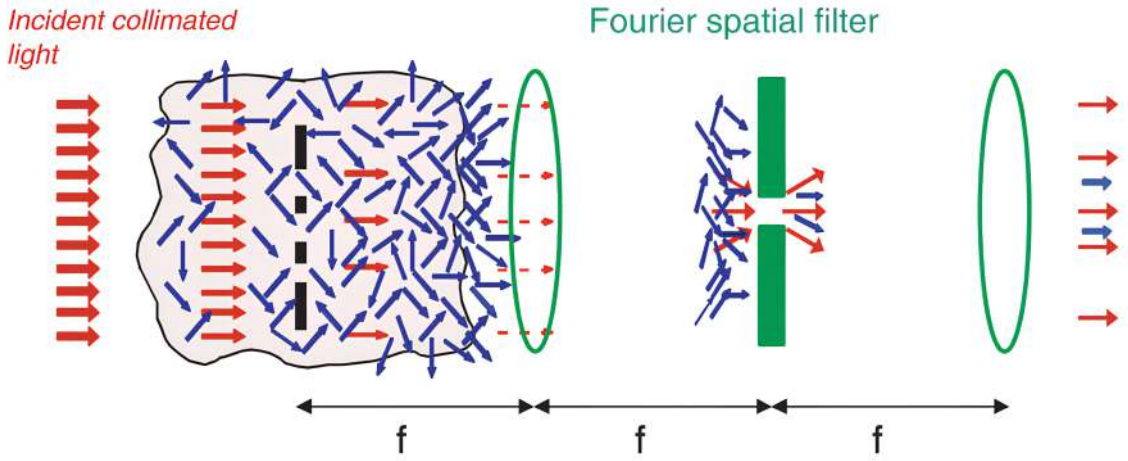

Fig. 1.9. Spatial filtering by Fourier plane spatial filter. The image is taken from Ref. [3].

to image an object embedded in a turbid media. This technique has greater resolution than whole-field techniques. Imaging trough turbid media using confocal scanning in transmission, and reflection scenario is shown Fig. 1.10.

Since ballistic photon arrive at the other side of any scattering medium earlier than the diffused photon, it is immediately apparent that time-gating offers a way to discriminate the ballistic photon against scattered light. In transmission scenario, ballistic photons always take the shortest route. Since the pulse width for ballistic signal is very narrow ($\sim$ 1 ps), it requires temporal discrimination faster than that. Time-gating can be performed using coherence of

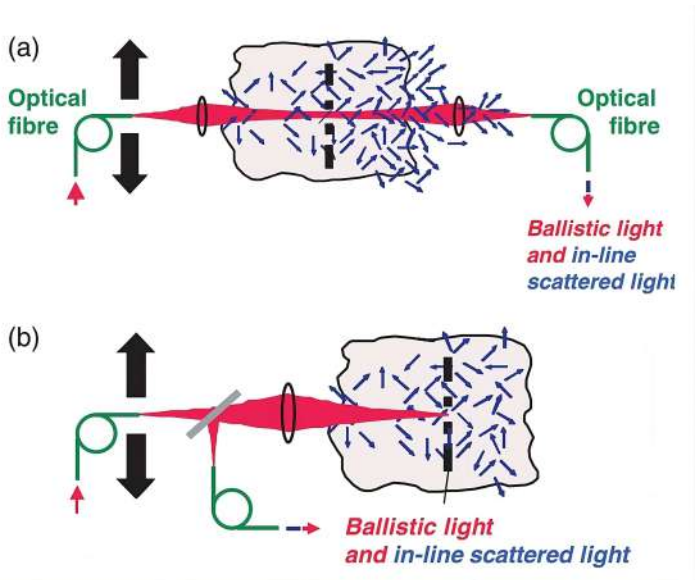

Fig. 1.10. Scanning confocal imaging (a) transmission and (b) reflection. The image is taken from Ref. [3].

the light or also incoherently. Incoherent time-gating can be realized by different techniques by using fast electronic devices such as streak camera, fast avalanche photodiodes, etc. It can also be performed by using nonlinear optical gates such as harmonic generation [11],

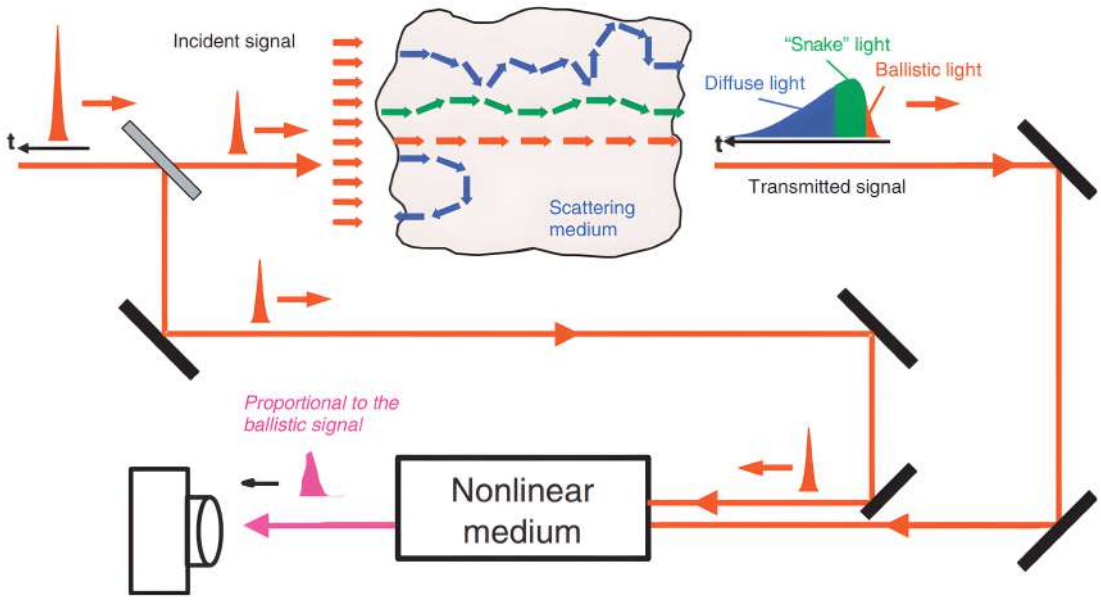

Fig. 1.11. Incoherent time-gated imaging technique using a nonlinear medium. The image is taken from Ref. [3].

parametric amplification [12], etc. One such general technique is shown in Fig. 1.11.

This discrimination against scattered light can be performed by coherent detection. This technique is widely described as Optical Coherence Tomography (OCT) [13], and are widely used in non-invasive bio-medical imaging of the eye and also tissue. A general schematic is shown in Fig. 1.12. These techniques can be found in great detail in Ref [3].

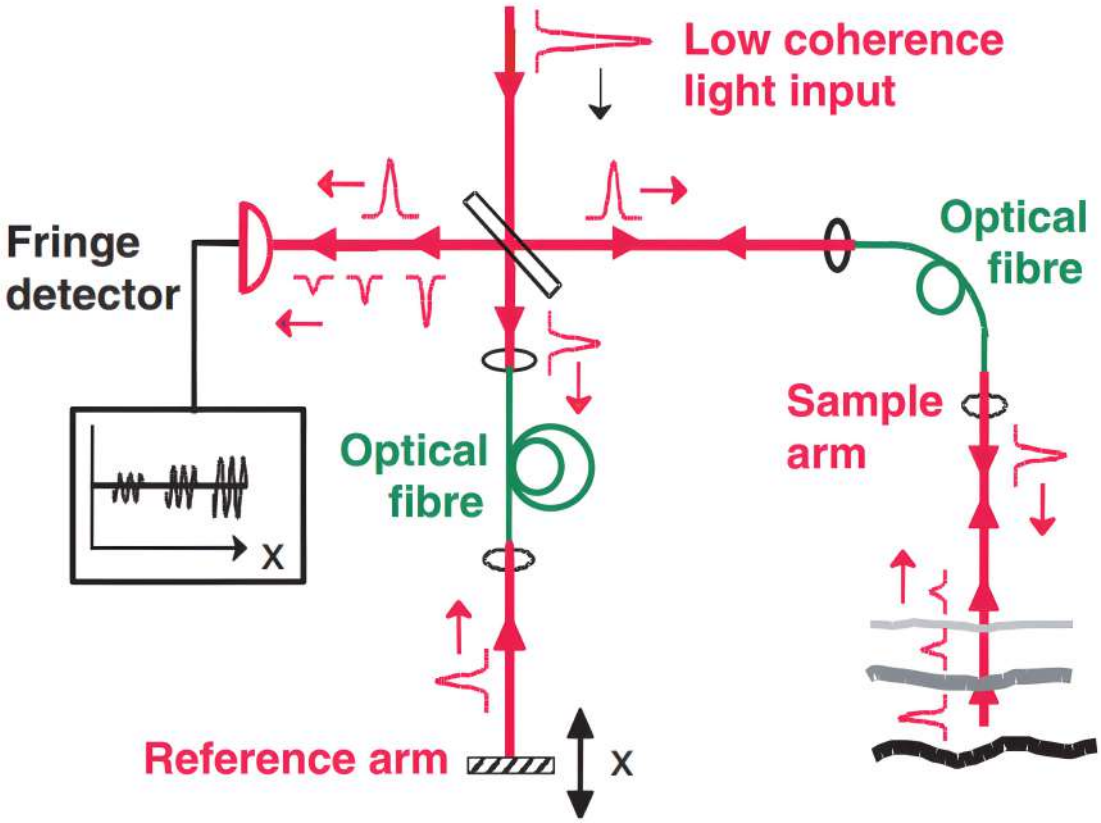

Fig. 1.12. Optical coherence tomography. The image is taken from Ref. [3].

A completely different technique, although uses the properties of light coming from different direction, tries to dehaze a single image using iterative algorithm [14]. This technique uses defogging algorithm which utilizes atmospheric light and airlight, and transmission map from the image. The implementation of the technique in the form of a block diagram is shown Fig. 1.13.

Apart from these, one technique uses a manipulated wavefront to focus the light on a particular point, which can then be imaged [15]. Hence, the technique is called the wavefront

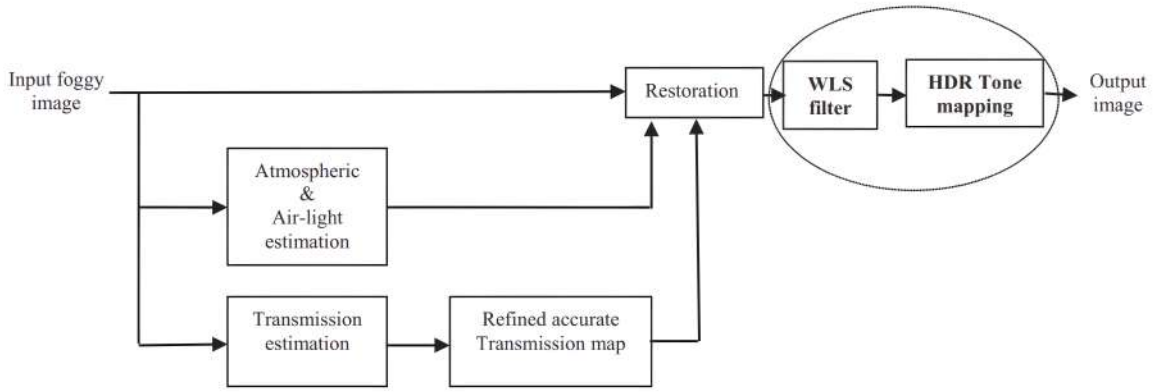

Fig. 1.13. Block diagram of a defog algorithm. The image is taken from Ref. [14].

shaping method. By manipulating the wavefront, all the phases of the waves can be interfered constructively at the particular point. We can understand this also using the time reversal property of light waves. If a light beam starts from a particular point and passes through a layer of turbid medium, the wavefront will have a complex structure. The same wavefront is needed to focus the light at the said point. The optimization of this process is achieved in an iterative way. The principle of the wavefront shaping method is shown in Fig. 1.14.

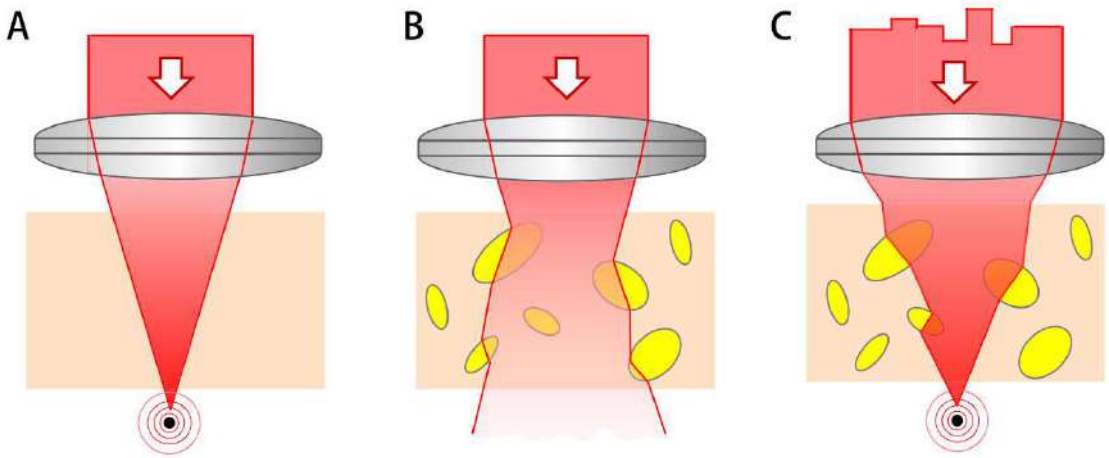

Fig. 1.14. Block diagram of a defog algorithm. The image is taken from Ref. [15].

Ballistic photons can also be filtered by encoding some information to the light signal and decoding it since these photons retain the signal properties. One simple approach to it is to modulate the light intensity and the demodulate it by lock-in technique, which can detect a

minute signal from a exceedingly noisy environment. In our work we used a technique similar to the lock-in technique, termed as Quadrature Lock-in Discrimination (QLD) technique. This technique is described in detail in Chapter 2.

1.6 Organization of the thesis

The thesis is organized as follows:

In **Chapter 1**, we give a brief introduction to the optical media, turbid media, scattering of light in turbid media, behaviour of photons in these media, and different types of imaging techniques using different types of photons.

In **Chapter 2**, we describe a detailed theory along with all the mathematics of the QLD technique. The performed simulation, the code, and simulated results are also mentioned.

In **Chapter 3**, we report a field application of imaging through fog. In this experiment, we image a modulated LED, as in beacons, at a distance of 150 m, in which the visibility was merely 50 m. Along with this we performed imaging of an illuminated white cardboard object. We also permed imaging of a particular source to distinguish it from other sources of light which can dazzle the viewer.

In **Chapter 4**, we present an enhancement of the contrast of the images obtained through fire and smoke. A blue LED and a blue filter are used in this technique. Fire is simulated using candle flame, and smoke is produced by a smoldering incense cone kept inside a chamber. The modulated light from the source travels through the flame and smoke, is reflected by the object, passes through the medium again, and is finally captured by a camera. After applying the QLD technique, we observe a significant improvement in the image contrast of the object.

In **Chapter 5**, we demonstrate a proof-of-principle imaging technique using an acousto-optic modulator (AOM). In this experiment, the demodulation of the QLD technique is done on an AOM as opposed to using the software. Using a series of frames, we saw a considerable enhancement in the image contrast. We also performed systematic imaging by varying camera parameters such as exposure time, frame rate, and the total number of frames to investigate its

effect on the improvement of the image contrast.

In **Chapter 6**, we summarize the essential observations and conclusions drawn from the experiments reported in this thesis, followed by the future prospects of the work.

Chapter 2

Quadrature lock-in discrimination

2.1 Introduction

The lock-in discrimination technique measures the amplitude of a signal buried in the noise by multiplying the noisy signal with a reference signal of the same frequency, followed by integration over a few cycles and finally tuning the reference to remove the relative phase factor, similar to a lock-in amplifier. The amplifier generally employs two sinusoids, the reference signal, and a quadrature sinusoid, to overcome the phase problem [16, 17]; hence, the technique is known as quadrature lock-in discrimination (QLD). After multiplying the noisy signal by the two sinusoids, sine and cosine, respectively, and integrating over many cycles,

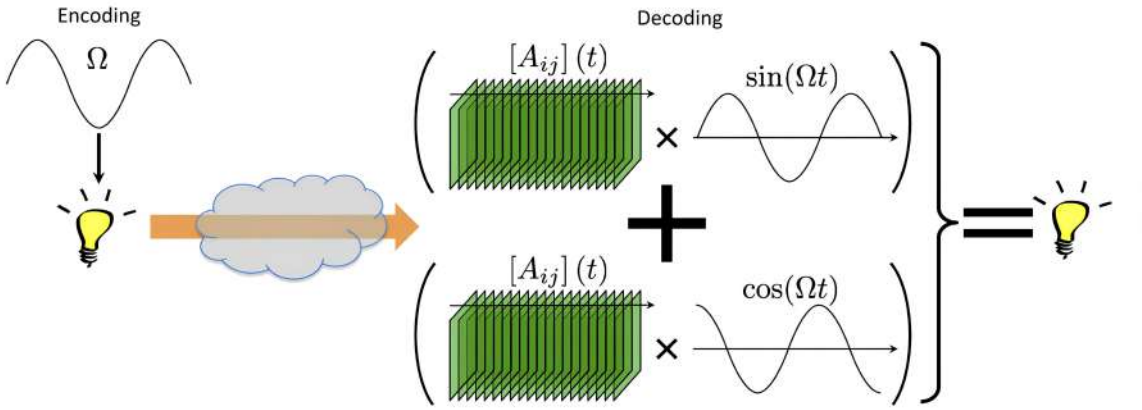

Fig. 2.1. Schematic presentation of QLD technique.

the amplitude and the phase can be easily extracted. So, in the first part of the technique, we encode our information using the intensity modulation, and decode or retrieve our information using the 'demodulation' technique applied on the received signal. The QLD technique improves the signal-to-noise ratio of the signal, which ultimately increases the contrast in the image. Fig. 2.1 illustrates a schematic explanation of the QLD technique. In our experiment, the data are recorded as 2D snapshots of the scene over time by an sCMOS camera, and the QLD algorithm is applied to all the pixels of a set of images using a MATLAB program. The corrected values of all the pixels are then replotted as an image to reveal the hidden/masked object [18].

2.2 Principle of operation

Imaging can be accomplished in two different geometries, namely, (i) transmission geometry and (ii) reflection geometry. As the name suggests, in transmission geometry, light from the source propagates through the turbid medium, and the camera collects the transmitted light. Although the light source can act as an object itself (e.g., runway lights, railways and roadways signals, etc.), the situation can be such that an external object is present between the light source and the medium i.e., shadow imaging. In the transmission scenario, the light source and the camera are placed on opposite sides of the scattering medium. Conversely, in the reflection geometry, the light source and the camera are placed on the same side, and the object is located on the other side of the medium. The light from the source travels through the scattering medium, which is reflected by the object, passes through the medium again, and is ultimately captured by the camera.

2.3 Theory

For a light source (such as an LED) that is modulated sinusoidally, the intensity of light can be written as,

$$S = A + B\sin(\omega t + \phi_0) \tag{2.1}$$

where A and B are the offset and amplitude, respectively, ω is the angular frequency, and ϕ_0 is the phase of the modulation. The ballistic photons, after passing through the turbid medium, retain the properties such as modulation frequency and phase, with a reduction in intensity. The intensity of the ballistic photons is given by,

$$s = a + b\sin(\omega t + \phi) \tag{2.2}$$

where a and b are the reduced offset and amplitude, respectively, and ϕ is the new phase of the modulation at the detector. Note that, although ballistic photons retain the phase, one might start detecting it at a different time, introducing a phase difference.

Now, multiplying Eq. (2.2) by $\sin(\omega t)$ and $\cos(\omega t)$, respectively, and integrating over a few cycles (from 0 to NT, where N is the number of cycles and T is the time period of the modulation, i.e., $T = 2\pi/\omega$), we will get,

$$q_1 = \frac{b}{2}NT\cos\phi, \tag{2.3}$$

and

$$q_2 = \frac{b}{2}NT\sin\phi, \tag{2.4}$$

where q_1 and q_2 are known as in-phase and quadrature components. A phase θ can be added in the reference signal, e.g., $\sin(\omega t + \theta)$. This gives $(\phi - \theta)$ in place of ϕ in Eqs. (2.3) and (2.4) as expected since phase is relative.

After squaring and adding the in-phase and quadrature components, b can be written as,

$$b = \frac{2}{NT}\sqrt{q_1^2 + q_2^2}. \tag{2.5}$$

This is the amplitude of the ballistic modulation. By plotting these values for all the pixels,

the image is obtained. An increase in intensity means more number of photons striking the medium. Hence, more ballistic photons will emerge from the medium, increasing the 'b' values. This will lead to an increase in the signal-to-noise ratio or contrast of the image. The implementation of the QLD technique using Eqs. (2.1) to (2.5) in the form of a block diagram is shown in Fig. 2.2.

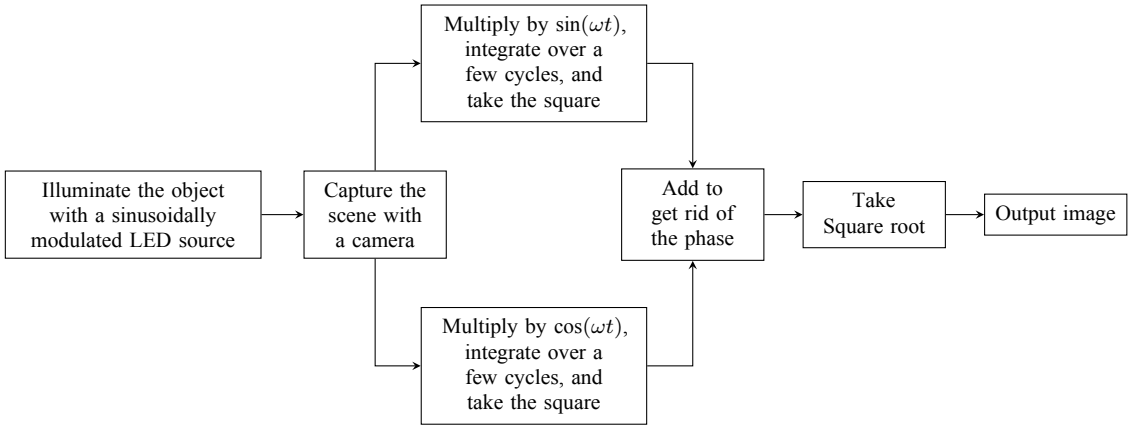

Fig. 2.2. Block diagram of QLD technique.

The offset value, 'a', should, in principle, reproduce the details about the original image, as spatial information of the scene is also being encoded in the offset value as in the amplitude 'b' of the signal, since both are reduced by the same amount due to the turbid media. However, due to the presence of noise, obtaining the DC component is difficult. Hence, we ignored the offset value in our calculation since only the amplitude value is sufficient. We also eliminated the phase as that is also not required.

Now, we can ask the question of what will happen if the signal is demodulated at some other frequency. To check this, let's multiply Eq. (2.2) by $\sin\omega' t$, and integrate over a few cycles (from 0 to NT', where N is the number of cycles and T' is the time period of the demodulation frequency, i.e., $T' = 2\pi/\omega'$), and we will get

$$q_1 = \frac{1}{2}Ab\frac{1}{(\omega-\omega')(\omega+\omega')}\left[(\omega+\omega')\sin\left(2\pi N\frac{\omega-\omega'}{\omega'}+\phi\right)\right.$$
$$\left.-(\omega-\omega')\sin\left(2\pi N\frac{\omega+\omega'}{\omega'}+\phi\right)-2\omega'\sin\phi\right] \quad (2.6)$$

and, similarly, for the q_2. Now, if we increase the N, these quadrature terms will vary sinusoidally and will not increase except when the two frequencies are the same according to Eqs. (2.3) and (2.4). Hence, the quadrature terms will be smaller compared to the case where the two frequencies are matched.

Now, in a real scenario, there will be noise along with the signal. The noisy signal can be written as the Fourier series of all frequencies present, ω_i's, with the corresponding sine and cosine amplitude a_i's and b_i's, as,

$$s_n = a_0 + \sum_i a_i \sin(\omega_i t) + \sum_i b_i \cos(\omega_i t), \tag{2.7}$$

where a_0 is the amplitude of the dc component.

Now, the same procedure as above can be applied to obtain the amplitude corresponding to the ω, as the contribution from the other frequencies to those two quadrature terms will be very less. Demodulating a signal at a frequency other than the modulation frequency results in a random, noisy image. This occurs because the contribution to the outcome from the modulation frequency is minimal, while noise frequencies within the signal contribute significantly. When multiple frequencies are present in the signal, demodulating at one of these frequencies will successfully retrieve the corresponding component. However, demodulating at any other frequency will produce a noisy image.

Since a camera captures the data in discrete frames, the integrations in Eqs. (2.3) and (2.4) are replaced by summations so that,

$$q_1 = \sum_t f_i \sin(\omega t) = \sum_i f_i \sin\left(2\pi\nu\frac{i}{\mu}\right) \tag{2.8}$$

and

$$q_2 = \sum_t f_i \cos(\omega t) = \sum_i f_i \cos\left(2\pi\nu\frac{i}{\mu}\right) \tag{2.9}$$

where f_i's are the discrete frames, and each frame contains a particular instance of the modulation along with noise, ν is the (linear) frequency of the modulation, and time (t) is

written as frame number (i) divided by the sampling frequency (μ). By using Eqs. (2.5), (2.8), and (2.9), the value of b is calculated. These numerical values are displayed as an image to obtain a noise-eliminated image of the object [18].

It should be mentioned here that turbid media parameters, such as particle density, particle size, etc., also affect the amount of scattering; hence, the amount of ballistic photons exiting the medium will change. A decrease in the number of ballistic photons needs to be countered with an increase in the light intensity up to a permissible limit in order to keep the SNR at an optimized value. In this sense, the modeling of the QLD technique does not directly depend on the turbid media parameters.

2.4 Algorithm to implement the simulation

To simulate the technique, we need to understand how a camera would capture a scene with modulated intensity. We could just multiply an image by a sine function to make it modulating, but it would not be exact as intensity can not be negative. To make it non-negative, we could just add 1 to it, but we need to multiply it by 1/2 to change the scale to '0 to 1'. After modulating the image, noise is added. The values are then multiplied by sine and cosine function of the same frequency, respectively. After each multiplication it should be added cumulatively to the sum of the previous terms, which is zero before the first frame. After that, the two terms need to be squared and added, and then the root is to be taken to find the amplitude of the signal. Finally, the scale needs to be changed to '0 to 1' to view it as an image.

2.5 Simulation

In this investigation, we first tried the simulation with a single image to check its viability. We would get the original image if it is demodulated at the same frequency as modulation, and a random image at the other frequencies. We also tried the same with two images, in

which one image is modulated at some frequency, and the other image is modulated at some other frequency.

2.5.1 Simulation with a single image

To verify our calculation, we simulate the QLD algorithm by using an image (Fig. 2.3(a)). We sinusoidally modulate the image at 13 Hz by multiplying the image with a sine function. A prime number is chosen as the modulation frequency, so that it doesn't interfere with the frequencies we encounter in our daily life, e.g., 50 Hz AC line, or multiple of it, while doing the experiment. We select the sampling frequency to capture the data, also known as frame rate, as 260 Hz so that there are 20 frames in a cycle of the modulation. We need a series of data taken over time for the QLD technique, and for that, we choose 13000 number of images. Finally, we mimic the noise by adding random numbers uniformly distributed between 0 and 1 to all the pixels of every frame. The intensity of the noise is chosen 10 times more than that of the signal to simulate a dense medium, making the scale of the noise is 0 to 10. The noisy

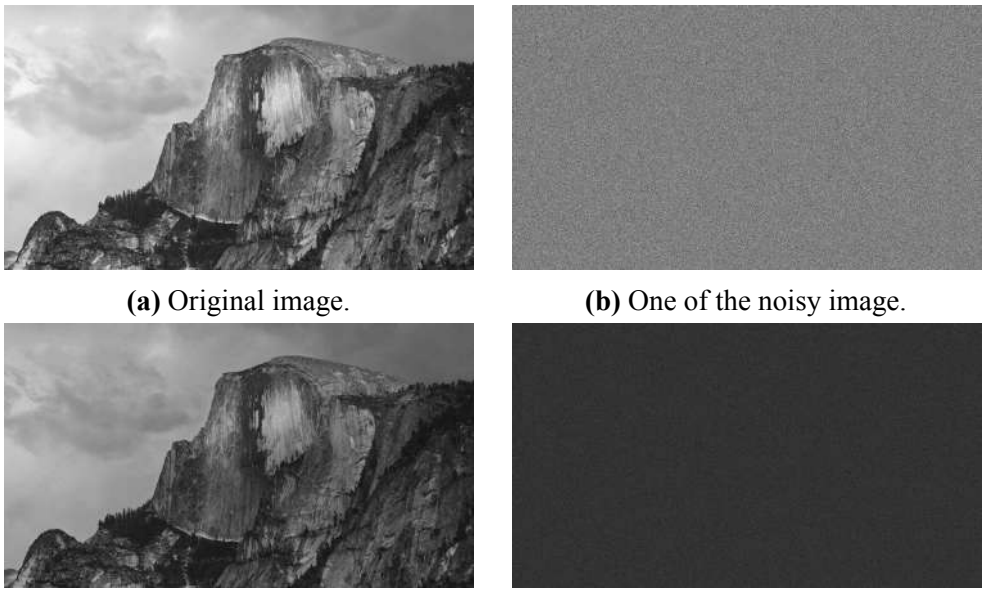

(a) Original image.

(b) One of the noisy image.

(c) QLD performed at the same frequency as the modulation.

(d) QLD performed at some frequency other than the modulation.

Fig. 2.3. Simulation of the QLD algorithm. Image Courtesy: (a) Internet.

images represent the raw frames that a camera would record of the intensity-modulated scene through a scattering medium. One such simulated raw frame is shown in Fig. 2.3(b). Clearly, the original image of Fig. 2.3(a) is not visible. We then apply QLD in order to retrieve the original image from the series of raw images. The original image is retrieved, with the added noise being filtered out, when processed at the same frequency of the modulation (13 Hz), and is shown in Fig. 2.3(c). On the other hand, QLD performed at some frequency other than the modulation (14 Hz), couldn't reveal any information of the original image and shows a random noisy image, and is shown in Fig. 2.3(d). The exact code of the simulation is given in Appendix A.

2.5.2 Simulation with two images

To check the simulation in a little more rigorous way, we use two images instead of one single image which are shown in Fig. 2.4(a,b). The first image is modulated at 13 Hz and the second image at 17 Hz, simultaneously. In this case, we need to choose the frame rate in such a way that for both modulations there is an integer number of frames. So, if we choose the frame rate as 221 (= 13 × 17) frames per second, it will be 17 frames per cycle for 13 Hz modulation, and vice versa. To take a long series of data, we choose a total number of 11050 frames. All other procedures are kept the same, like adding the offset and noise. Similarly,

(a) First image. **(b)** Second image. **(c)** One of the noisy image.

(d) QLD performed at 13 Hz. **(e)** QLD performed at 17 Hz. **(f)** QLD performed at 14 Hz.

Fig. 2.4. Simulation of the QLD algorithm. Image Courtesy: (a) Internet.

as above, we can see that the raw frame is a random noisy image (Fig. 2.4(c)), and neither of the original images, i.e., Fig. 2.4(a,b), is visible. In order to recover the images we need to apply the QLD technique at the corresponding frequencies. The results of processing the QLD at 13 Hz, and 17 Hz, are shown in Fig. 2.4(d,e), respectively. Again, the original images are retrieved, with the added noise being filtered out. Also, QLD performed at a "wrong" frequency (14 Hz) reveals neither of the images (Fig. 2.4(f)). The exact code of the simulation is given in Appendix A.

Chapter 3

Imaging through fog

Imaging through fog is a long-standing problem in scattering because fog hinders the imaging of an object through it by reducing visibility. In this chapter, experiments conducted in the field in the presence of fog, aimed at better imaging under poor visibility are reported. By means of intensity modulation at the source and two-dimensional quadrature lock-in detection by software at the receiver, a significant enhancement of the contrast-to-noise ratio was achieved in the imaging of beacons over hectometric distances. Further, by illuminating the field of view with a modulated source, the technique helped reveal objects that were earlier obscured due to multiple scattering of light. This method, thus, holds the promise of aiding in various forms of navigation under poor visibility due to fog.

3.1 Introduction

Visibility is reduced in fog because the tiny droplets of water suspended in air cause random multiple scattering of light, thereby degrading the image-bearing capabilities of photons. This is detrimental to many imaging applications of optics in open air, based either on passive imaging of scenes immersed in fog, or on active detection of beacons. This latter situation is of particular relevance when series of beacons are installed along runways to guide aircraft for landing and takeoff. It becomes impossible for the pilot to observe these

beacons during thick fogs, and there is no other alternative in the case of airfields or aircraft not equipped with radio-frequency instrument landing systems. Similar problems exist in maritime navigation, railway transportation, and even for motor transport on highways. Such examples illustrate the need for a simple, cheap, and compact technique aimed at improving the visibility of optical beacons in foggy weather conditions, and if possible also viewing objects that do not themselves emit light.

One class of "fog-removal" techniques is purely computational, where image processing algorithms are used on single or multiple images to remove the effect of fog (e.g., [14] and references therein). The other class of techniques exploits the physics of the problem and discriminates between different types of photon trajectories. Photons transiting a scattering medium are usually classified as (a) ballistic photons, that are forward scattered and retain their original direction of propagation, (b) snake photons, that are near forward scattered, and have paths that are not far from the ballistic, and (c) diffusive photons that are scattered through random angles over all directions and whose paths are scrambled such that the original direction of propagation is lost. The various approaches that have been used either select the small amount of ballistic (and snake) photons from among the huge amount of multiply scattered light that reaches the detector or the camera, or exploit the diffusive light itself to gain imaging capabilities [3, 19]. As illustrations of the first strategy, the ballistic photons may be temporally discriminated using a pulsed source of light in conjunction with time-gated detection [20] or time gated holography [21]. An alternative technique also based on pulsed laser illumination exploits the different statistics of backscattered and reflected photons [22]. Many recent works have aimed at imaging or focusing light through strongly scattering media, mainly for bio-medical imaging through live tissues [23–25]. These techniques, that characterize the scattering properties of the turbid medium, have limited applicability to fog, as the scatterers in fog are constantly moving at high speed.

In the context of imaging through fog, another simpler and cheaper approach consists in using a modulated continuous-wave source of light and relies on the fact that the intensity variation of the ballistic photons retains a phase relationship with the intensity modulation of the

source, while that of the multiply scattered photons does not. This technique requires a demodulation of the detected signal at the modulation frequency. Thus, the modulation-demodulation technique has proven to be efficient in enhancing source visibility, by discriminating against the background contributed by ambient lighting, sources modulated at different frequencies, and to varying extents, the diffusive photons. The demodulation may be performed using a bucket detector followed by lock-in electronics. This requires a step scan of the detector to build a two-dimensional image [26], and is thus time-consuming. Demodulation may be performed numerically using Fourier transform over a time-series of images [27]. Though many optimized algorithms are available for fast Fourier transform, the technique has its drawbacks [18] - it requires large memories to store the time series (1K frames or more) of images (each megapixels or more), on-camera buffer sizes are not large enough, and storage and read-out of images on the computer takes time. An alternative technique that was recently demonstrated consists in performing this demodulation instantaneously by optical means, with promising perspectives of high-frequency operation [28]. This, however, comes with increased complexity and cost of the optical elements. A different and simpler approach, suited for moderate frequencies, has also been recently demonstrated [18]. It consists in performing quadrature lock-in discrimination (QLD) [17] computationally to obtain real-time demodulation of images. By multiply-and-accumulate operation on each image as it is acquired, the need for storing a series of images is eliminated. By multiplying by the two quadratures of the modulation, the need for phase matching between the source and receiver is obviated. Exploiting the task and data parallelization capabilities of present-day desktop computers, this technique has been shown to lead to real-time display of 600×600 pixel images with low latency and at rates faster than the eye bandwidth. However, till now, this technique has been applied only in table-top experiments where suspensions of microspheres were used as the scattering medium. The aim of the present chapter is to test this technique in actual field conditions in “real” fog.

Here, we study the imaging of an light source, like as a beacon, in the transmission geometry, imaging of an object that illuminated by a modulated light source place closed

to it, rather than the source of light itself, as in reflection geometry, and also imaging of an modulated beacon in daylight condition to distinguish it from surrounding sources.

3.2 Theory and calculation

Although, the theory and calculation of the technique is already presented in Chapter 2, it would be helpful to describe it briefly. After propagating through fog, the noisy signal is captured by a camera over time. In our case, the data is captured as 2D snapshot as in a wide-field imaging. So, experimentally, we would record noisy frames, f_i's. After capturing the data, the QLD technique is employed to every pixel of the image by using the Eqs. (2.5), (2.8), and (2.9) to obtain a noise-eliminated image of the object. The exact code of the simulation is given in Appendix B.

3.3 Experiments

We performed experiments in three different scenarios. (i) Imaging of an modulated light source, (ii) Imaging of an object illuminated by a modulated light source place closed to it, and (iii) Imaging of a particular object in a daylight condition to distinguish it from unwanted objects.

3.3.1 Application of QLD to a modulated beacon

To test the efficiency of QLD in real fog, we performed field experiments as schematized in Fig. 3.1, over a period of two months during peak winter at Shiv Nadar University, Uttar Pradesh. A LED panel, consisting of 10 uncollimated LEDs connected in parallel on a 10 cm $\times$ 16 cm standard printed circuit board, emitting typically 1 Watt each in the red (around 640 nm), was used as the source of light. Several factors, apart from the ease of availability of LEDs, contributed to this choice of wavelength. Red light is conventionally used to signify danger, and most warning lights are in this colour. Further, the Rayleigh scattering of light

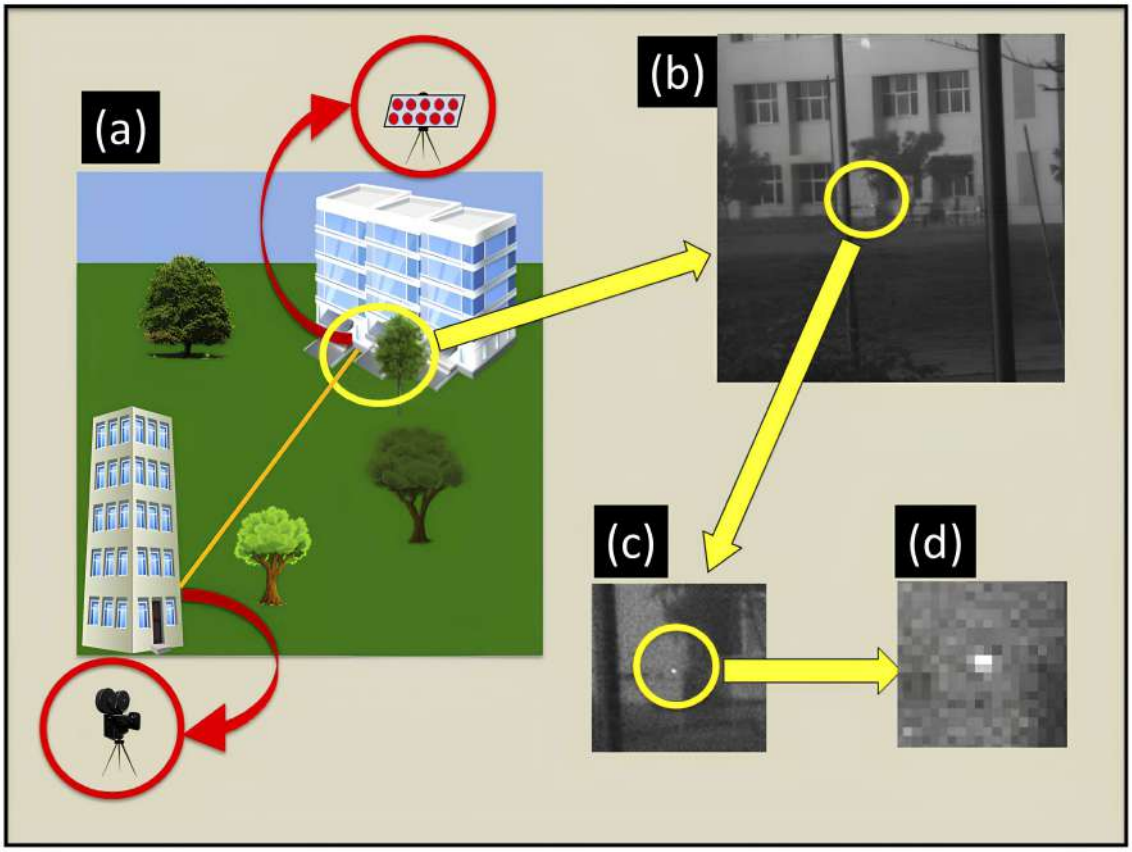

Fig. 3.1. Schematic of the experiment. The red curved arrows indicate the location of the camera in the building in the foreground, and the LED panel fixed on the building at the background. The distance between the two is 150 m; the orange full line indicates the clear line-of-sight between them. (b) An image of a portion of the building housing the LED panel, as captured at daybreak, in the absence of fog. The portion circled in yellow is enlarged and shown in (c); this is further enlarged and shown in (d). The processed images appearing in later figures may be compared with (d).

is proportional to the inverse fourth power of wavelength, and therefore the red part of the spectrum should be preferred over the blue. Finally, most cameras have the highest sensitivity in this part of the spectrum. The entire bunch of LEDs were so closely spaced that they could not be individually resolved at the camera, and thus appeared as a single bright source. The current through the LEDs was modulated (peak-to-peak modulation amplitude equal to 30% of the average current) so that the intensity of the emitted light could be varied sinusoidally at any frequency in the range 13 - 17 Hz. The detector used was a 16-bit Andor Neo sCMOS camera, controlled by Andor Solis software, with a 8-48 mm F/1–1.2 zoom lens from Ernitec.

In the conditions of our acquisitions, the actual pixel dynamic of the camera is 13.4 bits, obtained from the ratio of the pixel well depth (30000 electrons) to the RMS read noise (2.8 electron according to the manufacturer). Series of frames of the scene at the desired frame rates were acquired and transferred to a desktop computer where they were processed for the extraction of images using the QLD technique. The distance between the source and the detector was 150 meters. We used natural features of the scene to evaluate visibilities, which during our acquisitions, ranged between 30 to 150 m.

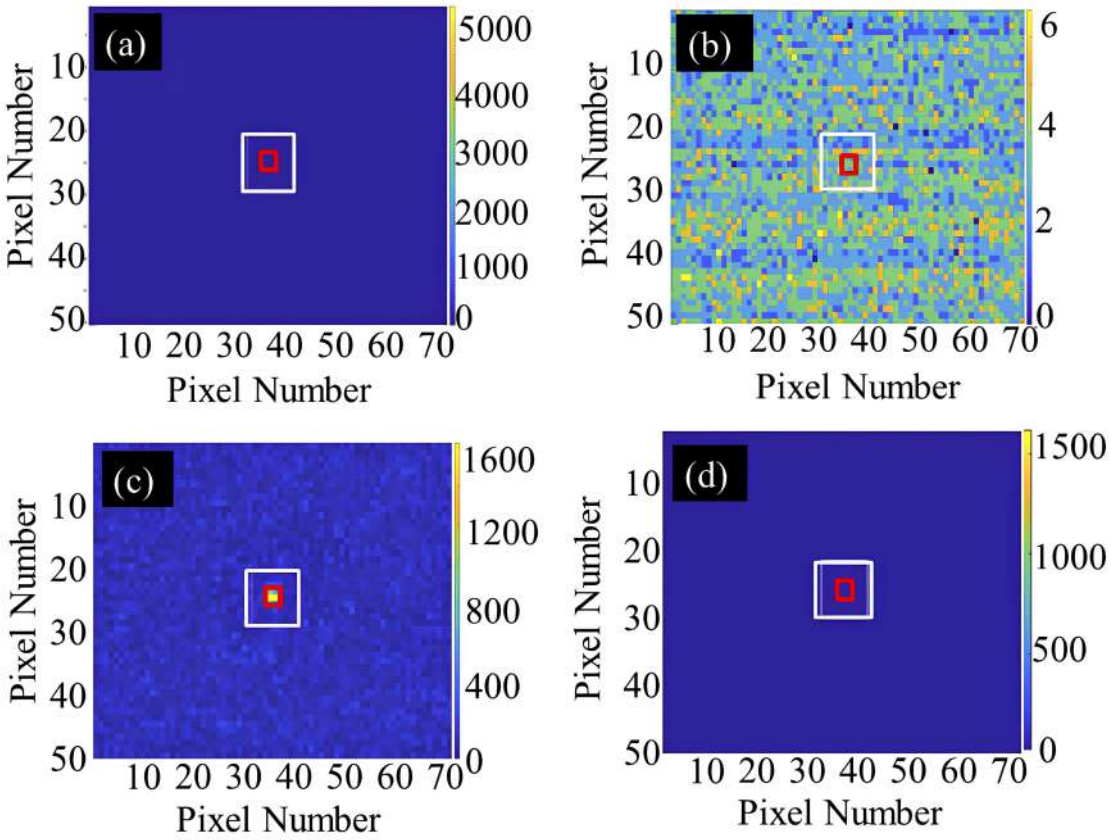

Fig. 3.2. Examples of raw and QLD-processed images acquired at day-break with a visibility of 40 m. (a) One full-scale raw frame (CNR = 2.3, 1 ms exposure time). (b) Same as (a) for a reduced color scale. (c) Corresponding processed image obtained from 10140 raw frames acquired at 390 frames per second. CNR is now equal to 11.0 (d) The image obtained by averaging all 10140 raw frames. The source is not seen, the CNR is 2.5. The red and the white squares in the figures represent the "object" and the "background" regions defined after Eq. 3.1.

In Fig. 3.2 we describe a set of recordings made when the source was modulated at 13 Hz.

Each data set was based on the acquisition of a total of 10,140 frames collected at rates of 260 or 390 Hz, and with exposure times per frame ranging from 0.5 ms to 5 ms depending on the weather condition. A raw frame recorded in one of the experiments is shown in false colour in Fig. 3.2(a). Although this frame was acquired at day-break, the LED panel, located at a distance of 150 m, is not visible because of the heavy fog conditions with visibility of 40 m. This frame is re-plotted in Fig. 3.2(b) with a different colour scale corresponding to a scale enhancement by a factor 850. The LED panel is still almost impossible to distinguish. After QLD processing of 10,140 such raw frames, we obtain the result reproduced in Fig. 3.2(c), where, in contrast to Fig. 3.2(a,b), one can now clearly see the LED panel at the centre. Fig. 3.2(d) shows the image obtained upon averaging the 10140 raw frames, without QLD processing. The source is not visible in this case.

In order to gain a more quantitative picture of the improvement of the image quality obtained using QLD, we measure the Contrast-to-Noise Ratio (CNR), defined as:

$$\mathrm{CNR} = \frac{\langle I_{\mathrm{obj}} \rangle - \langle I_{\mathrm{back}} \rangle}{\left\langle \left(I_{jk} - \langle I_{\mathrm{back}} \rangle \right)^2 \right\rangle_{\mathrm{back}}^{1/2}}. \tag{3.1}$$

In this expression, $\langle I_{\mathrm{obj}} \rangle$ is the average value of the signal over the pixels covering the modulated source. In the case of Fig. 3.2, it corresponds to the 3×3 pixels surrounded by the red rectangle. The quantity $\langle I_{\mathrm{back}} \rangle$ is the average of the signal recorded in the background surrounding the object. In Fig. 3.2, it corresponds to the 8 blocks of 3×3 pixels contained in the white rectangle. In the denominator, the averaging is taken over the same i, j pixels belonging to the surrounding background, so that this denominator is the square root of the variance of the background noise.

For the data of Fig. 3.2 (visibility 40 m) QLD applied to images acquired at a distance of 150 m from the source permits to increase the CNR from 2.3 to 11. In Fig. 3.3, we plot the evolution of the CNR as a function of the number of cycles over which QLD averaging is performed. The results in this figure, obtained in five sets of experiments performed at day-break for visibilities ranging from 40 to 60 m, show that the CNR can be significantly

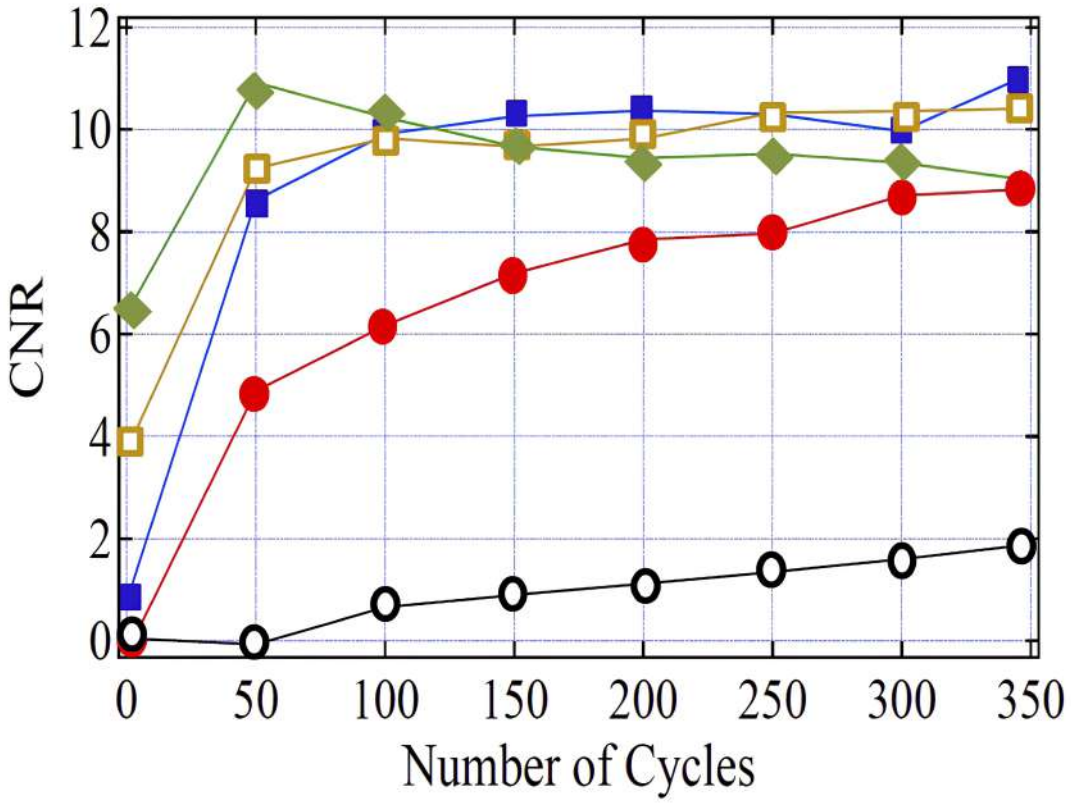

Fig. 3.3. Evolution of the CNR as a function of the number of processed modulation cycles. Modulation frequency = 13 Hz; 390 frames per second. Full circles: 40 m visibility; 1 ms exposure time. Full squares: 40 m visibility; 1 ms exposure time. Full diamonds: 50 m visibility; 2 ms exposure time. Open circles: 60 m visibility; 1 ms exposure time. Open squares: 60 m visibility; 0.5 ms exposure time.

increased using the technique of QLD. Four of them permit to reach a value of the CNR larger than 8, typically with the number of periods needed to optimize the CNR being of the order of 100. While the general trend for all data sets is the same, variations exist. For example, the curves shown in full circles and in full squares, both of which are for a visibility of 40 m, are different. This may be attributed to the somewhat different nature of the fog on the two days the data was taken, or to possible variations of the ambient illumination. It is well known that fog can have droplets with sizes ranging from sub-micrometer to several micrometers [29], and thus the scattering can vary from being isotropic to significantly anisotropic (forward scattering), leading to a difference in the efficiency of the QLD technique. This effect is

more pronounced in the curve with open circles in Fig. 3.3, which is quite different from the other four: the CNR is initially close to zero, and increases very slowly as a function of the number of modulation cycles over which QLD is performed, reaching a modest value of 1.9 even when all the available data are processed. Though this set of data was not obtained for a visibility significantly lower than the other sets of data, the nature of fog varied during observation. The wind was relatively strong then, and fog trails could be seen passing across the scene, indicating that the density and diameter of the water droplets was changing with time during the acquisition time, thus leading to the different results for seemingly identical conditions. It is also quite possible that these variations in the fog during acquisition explains why, in the case of the data represented as full diamonds, the CNR slowly decreases when the number of cycles is increased above 100.

3.3.2 Application of QLD to an illuminated object

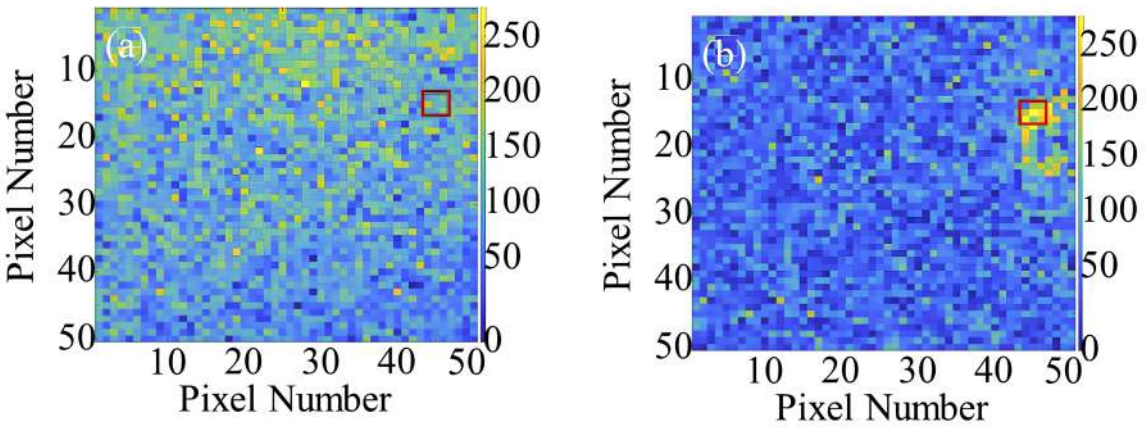

Fig. 3.4. Examples of raw and QLD-processed images acquired at day-break with a visibility of 30 m. The red rectangle shows the position of the piece of cardboard that is illuminated by the light of modulated LED panel. (a) One full-scale raw frame (5 ms exposure time). (b) Corresponding processed image obtained from 10,400 raw frames acquired at 160 frames per second. The modulation frequency is 16 Hz.

We have, so far, focused on imaging light beacons through fog using the technique of QLD. We now investigate whether this method can be used under foggy conditions to enhance the visibility of an object that is illuminated by the modulated source of light, rather than the

source of light itself. The data presented in Fig. 3.4 were obtained at day-break by illuminating using the modulated LED panel, a piece of cardboard located on the right of the picture. The distance between the LED panel and the illuminated cardboard was about 20 cm. The distance between this object and the camera was 75 m while the visibility through fog was estimated at about 30 m. In the raw frame of Fig. 3.4(a) the object cannot be distinguished; the associated CNR, equal to 0.3, is indeed quite low. However, after QLD processing of 10,400 such frames acquired at a rate of 160 images per second, the image of Fig. 3.4(b) was obtained, where the object illuminated by the LED panel can be clearly distinguished from the noisy background, with a CNR of 1.9. Notice that in the present experiment the QLD technique works at low modulation frequencies because the modulated light source is close to the illuminated object. Making it to work with the modulated light source close to the camera and thus far from the object would probably require much higher frequencies or even pulsed illumination.

3.3.3 QLD imaging in daylight condition

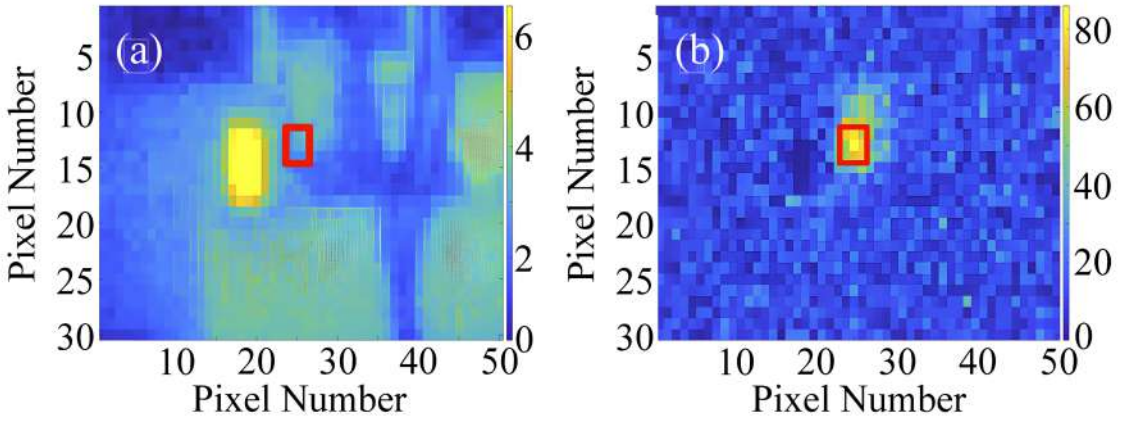

Fig. 3.5. Examples of raw and QLD-processed images acquired during day time. The red rectangle shows the position of the piece of cardboard that is illuminated by the modulated LED panel. (a) One full-scale raw frame (5 ms exposure time), showing reflection of sunlight from a polystyrene object located close to the LED panel (b) Corresponding processed image obtained from 10,400 raw frames acquired at 160 frames per second. The modulation frequency is 16 Hz.

The preceding results of Figs. 3.2 to 3.4 were obtained during daybreak, when the LED

panel was much brighter than the ambient light. We now show that QLD can also be useful in distinguishing a modulated beacon or an object illuminated by a modulated source, from surrounding sources of light, especially during day time when many objects can reflect the sun light and blind the observer. Fig. 3.5 illustrates this capability, using a similar setup as in Fig. 3.4, but obtained during day time fog. Here, only a cardboard piece is illuminated by the modulated light provided by the LED panel. Close to it, but shielded from the modulated source, is a polystyrene block that strongly scatters sunlight towards the camera. Both objects, the cardboard and the polystyrene block, are 150 m from the camera, and are viewed through fog during daylight. In Fig. 3.5(a), the parasitic sunlight reflection is clearly visible, while the illuminated cardboard is impossible to distinguish, as confirmed by a CNR measured to be equal to -0.3 for this image. This image also exhibits vague shapes in the foreground due to intervening trees. After QLD processing (see Fig. 3.5(b)), all these spurious shining objects disappear, and we are left with a clearly visible image of the piece of cardboard illuminated by the LED panel, with a CNR which is now equal to 2.4.

3.4 Summary

We have shown that computational QLD processing of images obtained using a modulated LED source is a powerful tool, compatible with real-time processing, which could be very useful for many applications. The fact that such imaging can be performed by illuminating with simple LEDs and processing on an ordinary computer shows that it can potentially be implemented at low cost, which further paves the way to a broad range of applications. In particular, this technique has been proven to be efficient in improving the visibility of beacons under heavy fog conditions, particularly at night, a situation that is commonly encountered during plane landing and takeoff. Moreover, we have shown that it is also capable of imaging a reflecting or diffusive object which is illuminated by the modulated source of light. Thus, in the context of aircraft navigation, unlike modern instrument landing systems that merely guide an aircraft using radio waves, the QLD technique can provide the pilot a visual image

of the scene that lies ahead, and in particular a realistic representation of the runway beacons. In motor, rail or maritime navigation, apart from showing the path by means of beacons, the technique may be used to reveal obstacles in the path, that are otherwise hidden by fog. The technique is particularly interesting if one wants to be able to steer the direction of emission of the modulated light, like in the case of a lighthouse, whose range could thus be extended in heavy fog conditions. Finally, we have shown that source modulation and QLD also proves to be interesting in the presence of daylight, because it permits one to distinguish the beacon or object of interest from any surrounding source of light that could dazzle the observer.

Chapter 4

Imaging through fire and smoke

Visibility is a big issue in imaging through fire and smoke, a situation often encountered by firefighters. Emission from fire is significantly higher in intensity compared to the light reflected from an object obscured by fire, leading to a drastic reduction in the signal-to-noise ratio for visualization. On the other hand, the presence of smoke scatters light in random directions, further reducing visibility. By implementing a quadrature lock-in discrimination algorithm on the images captured by an sCMOS camera in the presence of a modulated blue light source and blue filter, a significant improvement in the image contrast measured for an object in the presence of flame and smoke, is presented. Our methodology is straightforward to realize and facilitates the reliable identification of objects that are otherwise concealed in real-life situations due to poor visibility.

4.1 Introduction

Accidents involving fire cause loss of lives, injuries, and trauma to human beings that are irreparable. In India, according to the National Crime Records Bureau, more than ten thousand fires had been spread during the year 2019, causing approximately eleven thousand deaths [30]. In the USA, the number of fires is in the millions, causing 3700 deaths, according to the U.S. Fire Administration [31]. The firefighters have a mission to extinguish the fire and

search and rescue trapped human beings [32]. Unfortunately, the strong emission from fire generally masks the visibility of the humans and objects in its vicinity, both to our eyes and visible light-based camera. Moreover, the presence of smoke diffusely scatters the light in random directions, hampering direct imaging. An alternative to visible light-based imaging is to use an infrared part of the spectrum for imaging through smoke, which offers an advantage by minimizing the scattering effect during direct imaging [33–37]. However, the presence of fire completely changes the scenario and causes saturation of the camera. Although the saturation or blinding of IR detectors poses a severe constraint, a few methods have been reported to tackle this issue [38, 39]. There is a report that has demonstrated improved imaging using a lensless method such as holography using a 10.6 µm laser that avoids saturation of infrared detectors [40]. In a recent measurement using a laser-based heterodyne technique [41], concealed objects behind flames were monitored for alteration in their shape with an unprecedented precision of 30 µm at a distance of two meters. An automated neural network-based imaging in the infrared has been very recently reported to detect humans through a flame; however, the flame background could not be completely eliminated [42].

Even though visible light-based imaging has a considerable loss in visibility and poses a formidable challenge in imaging an object through fire and smoke, it is nonetheless economical. The availability of real-time "fire removed" images in the fire-affected zone is critical towards minimizing loss and fatalities in a rescue operation. The primary task being the reduction of strong background visible emissions from fire; however, there has been a paucity of experimental work in overcoming the visibility issue. In an earlier work, to reduce the background flame emission, a blue laser was used to measure target displacement in the close vicinity of flames produced by natural gas [43]. In a recent report by the same authors, the visibility of an object surrounded by fire was shown to enhance by not only using a blue light source but also by blocking the intense part of fire emission with a blue filter [44]. However, these imaging studies were performed in the absence of smoke. Optical imaging through smoke is a non-trivial task since the light signal experiences a significant attenuation that depends on the wavelength of light, particle size, and concentration.

Different approaches have been suggested [44] to improve the image quality of an object in the presence of fire. A CCD camera with onboard lock-in detection [45] that has the capability of performing measurements of amplitude, phase, and background at pixel level might be advantageous. Another approach based on well-known polarimetric imaging has been proposed for imaging through fire and smoke [44]. Polarimetric imaging through the atmosphere is well known [46–48]; however, it requires either a polarimetric camera or a normal camera with a polarizer. In the case of weaker scattering, such as haze, post-process algorithms [46, 47] for polarimetric imaging utilize the polarimetric data to dehaze a scene. In recent years, a new tabletop experiment to image an object through fog in real-time based on the quadrature lock-in discrimination (QLD) algorithm [18] has been demonstrated. It consists of a modulating light source that propagates through the scattering medium. The forward scattered, namely ballistic photons [1], retain the properties such as propagation direction, polarization, and phase. These photons are used to image the object after filtering out the multiply scattered diffused photons. The image sequences are recorded at a frame rate greater than the modulating frequency. The QLD algorithm that performs demodulation is applied to the raw image sequence, enhancing the visibility of hidden objects in real-time. The utility of this approach in imaging through fog has been recently extended to over a distance of 150 m [49]. Instead of the QLD algorithm, the demodulation has been recently demonstrated by all-optical hardware from a single frame [28]. However, it comes with additional optical complexities and increases the cost. The effectiveness of the QLD algorithm in improving imaging through fire and smoke scenarios is yet to be explored.

In this chapter, we show an enhancement in the visibility of an object imaged through both flame and smoke using a modulated blue LED light source, a blue filter, and the QLD algorithm. We performed the experiment first only with flame and then with both, flame and smoke. We also performed the experiment with white LED light source and blue filter. Finally, we performed the experiment with red LED light source and red filter.

4.2 Theory and calculation

Although, the theory and calculation of the technique is already presented in Chapter 2, it would be helpful to describe it briefly. After propagating through flame and smoke, the noisy signal is captured by a camera over time. In this case also, we would record noisy frames, f_i's. After capturing the data, the QLD technique is employed to every pixel of the image by using the Eqs. (2.5), (2.8), and (2.9) to obtain a noise-eliminated image of the object. The exact code of the simulation is given in Appendix C.

4.3 Experimental setup

The photograph of our experimental setup is shown in Fig. 4.1(a), and the schematic of the

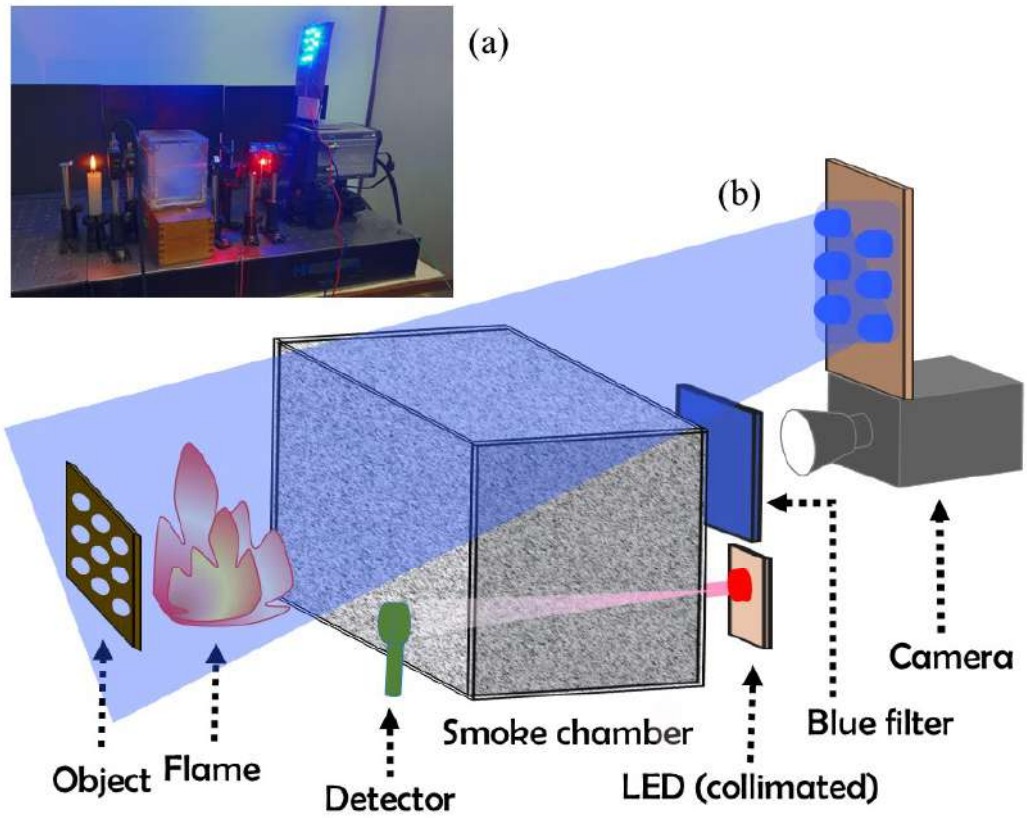

Fig. 4.1. (a) Photograph, and (b) Schematic of the experimental setup. Light from the blue LED panel illuminates the object and reflected light is detected by the camera with a blue filter. The red LED and detector are used for measuring the smoke density in the chamber.

same is shown in Fig. 4.1(b). The object is a 5 mm $\times$ 5 mm rectangle frame having nine holes of 1 mm diameter each, separated by a center-to-center distance of 1.5 mm. The modulating source is an LED panel, which consists of a parallel combination of 10 un-collimated LEDs emitting $\sim$ 1 W power each, stacked on a 10 cm $\times$ 16 cm standard printed circuit board. The LEDs are closely spaced so that they cannot be individually resolved and appear as a single bright source. The current flowing through the LEDs is modulated such that the emitted light intensity can be varied sinusoidally. The modulation frequency for the LEDs in our measurement is 13 Hz. The modulated LED illuminates the object, and the light reflected from the object reaches the camera (16-bit Andor Neo 5.5 sCMOS camera, controlled by Andor Solis software). The camera is equipped with an 8-48 mm F/1–1.2 zoom lens from Ernitec, and a blue filter (BG 12) is placed in front of the camera. Candles flame is used to simulate fire. The illumination light, as well as the reflected light, can be made to pass through a smoke chamber and candle flame as required. Smoke is produced by a smoldering incense cone kept in the chamber. Since, the incense cone is dying out, the smoke density was changing. The distance of the flame, smoke chamber, filter, and camera from the object is 3.8 cm, 12.7 cm, 27.9 cm, and 43.2 cm, respectively.

A series of frames are captured at different frame rates (26, 39, 52, 78, 104 Hz) and exposure times (0.01 ms to 5 ms) and are processed using the QLD algorithm. The frame resolution is $\sim$ 600 $\times$ 600 pixels. The limiting value of exposure time, frame rate, and the total number of frames depend on the frame resolution and computer and camera memory. We have used two different LEDs (blue and white) in our measurements. A separate red LED, whose transmission through the smoke chamber is monitored using a photodiode connected to an oscilloscope, is used to quantify the smoke density in our experiments. Also, we used red LED along with red filter.

4.4 Results and discussion

In this experiment, the blue filter is used to block most of the intensity in blue region.

Therefore, the spectrum of the LED light sources and the flame, with and without the filters, is determined first.

4.4.1 Optical spectrum of the LEDs and the flame with and without the filters

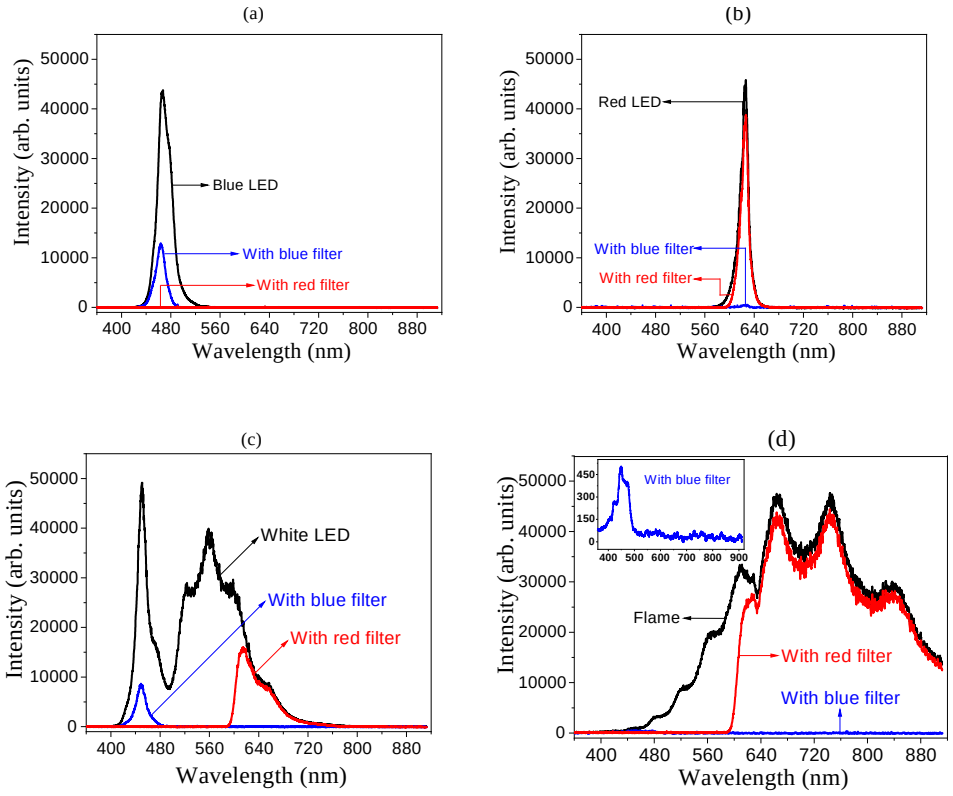

Fig. 4.2. Spectra of blue, red, and white LEDs (a-c) and spectrum of the candle flame (d), recorded with blue and red filters and also direct without the filters.

In Fig. 4.2(a), spectrum of the light from a blue LED without any filter, and measured through a blue filter and a red filter are presented. The black colour plot is the direct spectrum, i.e., without any filter of the blue light. The blue and red plots are the spectrum of the same with the blue and red filter, respectively. Similarly, in Fig. 4.2(b,c), the spectra of the red and white light is shown, respectively. The flame spectrum without any filter and transmitted through a blue and red filter is shown in Fig. 4.2(d), and the inset also shows rescaled graph of the flame spectrum measured with the blue filter. It should be mentioned here that the

arbitrary units used in the y axis in the four graphs for different light and flame are different. The fire intensity is much more than that of the light sources. The acquisition time is kept such that the maximum counts is less than the 90% of the full ADC scale, which is approximately 59000 counts for 16bit ADC. The values are kept around 50000 counts in our experiment so that it does not even touch the 90% limit. Also, it should not be too low so that it looks like more fluctuative. Hence, the acquisition time for the flame spectrum is less than that for the LED light sources so that the maximum counts for all the spectra is same ($\sim$ 50000). The spectra are measured using an Avantes multichannel spectrometer having five channels. The spectral range for the channel used is 360 nm to 910 nm.

From Fig. 4.2(d), we can see that the intensity of the flame in the blue region is one order less compared to the other parts (green, red and infrared) of the spectrum. Also, from the Fig. 4.2(c) it is evident that the blue filter transmits lights with some transmission efficiency, and blocks almost all the lights in the region other than blue. Therefore, using a blue filter will significantly reduce the high intense background noise from the fire [44]. Hence, to perform the measurement, we use blue light having wavelength in the bandwidth of the filter. One might think that blue light might not be beneficial, as it will be far more scattered than any other part of the visible spectrum. This dependence occurs in the Rayleigh regime, where the size parameter, defined as, $x = 2\pi r/\lambda$, is much less than unity, or correspondingly, the radius of the scatterer (r) is at least one order lower in magnitude than the wavelength (λ) of the light. The wavelength of the blue LED light source used here is 467 nm, whereas the size distribution of the smoke particles generated from a smoldering incense cone ranges from $\sim$ 10 nm up to a few micrometers, with a peak particle density at $\sim$ 100 nm [50–52]. Although, a few of these particles fall on the Rayleigh scattering regime, the majority of the scatterers fall on the overlapping region and Mie scattering region. In these two regions, the scattering is almost same for blue and red wavelength. In addition, the sCMOS camera used in our measurement has a quantum efficiency (QE) of $\sim 50\%$ at 467 nm, which is close to that at the red region, where the QE is maximum ($\sim 58\%$). Lastly, the LED based light source used is lightweight and low cost. For these reasons, we have used blue LED, blue filter

combination in our experiments. We have also used white LED, blue filter and red LED, red filter combination to check and compare the results.

4.4.2 Imaging experiment with blue light and blue filter combination

Imaging with flame

We present two sets of images: one captured with only the flame, and the other with both flame and smoke chamber, in the beam path. The images are captured using the blue LED light source with a blue filter in front of the camera. In Fig. 4.3, we show a comparison of raw and processed images of the object in the presence of flame (using three candles) as a function of different exposure times. It is evident from the figure that in the absence of the blue

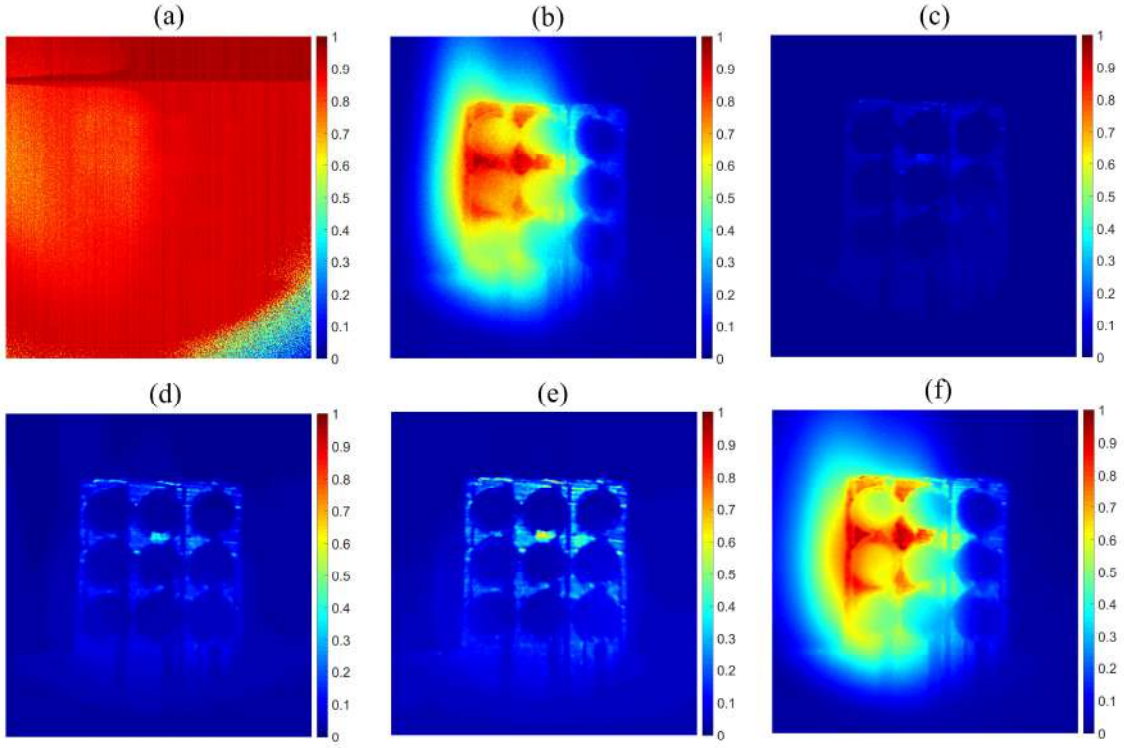

Fig. 4.3. Comparison between the raw and processed images captured for different exposure times with blue light and blue filter in the presence of flame. (a) Saturated raw image of the object. (b) Image after adding blue light and blue filter combination. (c-e) Processed images using QLD algorithm for exposure times of 1 ms, 3 ms, and 5 ms, respectively. (f) Average of all the raw frames used for processing, for the exposure time of 1 ms.

filter, we observe a saturated image of the flame with no visibility of the object (Fig. 4.3(a)). When the blue light and blue filter combination is used, the saturation is significantly reduced; however, the object is still not clearly visible (Fig. 4.3(b)). By applying the QLD algorithm to the captured images, keeping the frame rate (91) and the total number of images (455) constant, we observe a significant improvement in the visibility of the object (Fig. 4.3(c-e)), which increases with increase in the exposure time (for exposure times of 1 ms, 3 ms, and 5 ms, respectively). Instead of processing the frames using QLD, if we take the average of all the 455 raw frames, no improvement in the visibility of the image is observed (Fig. 4.3(f)), bringing to the fore the importance of the QLD technique.

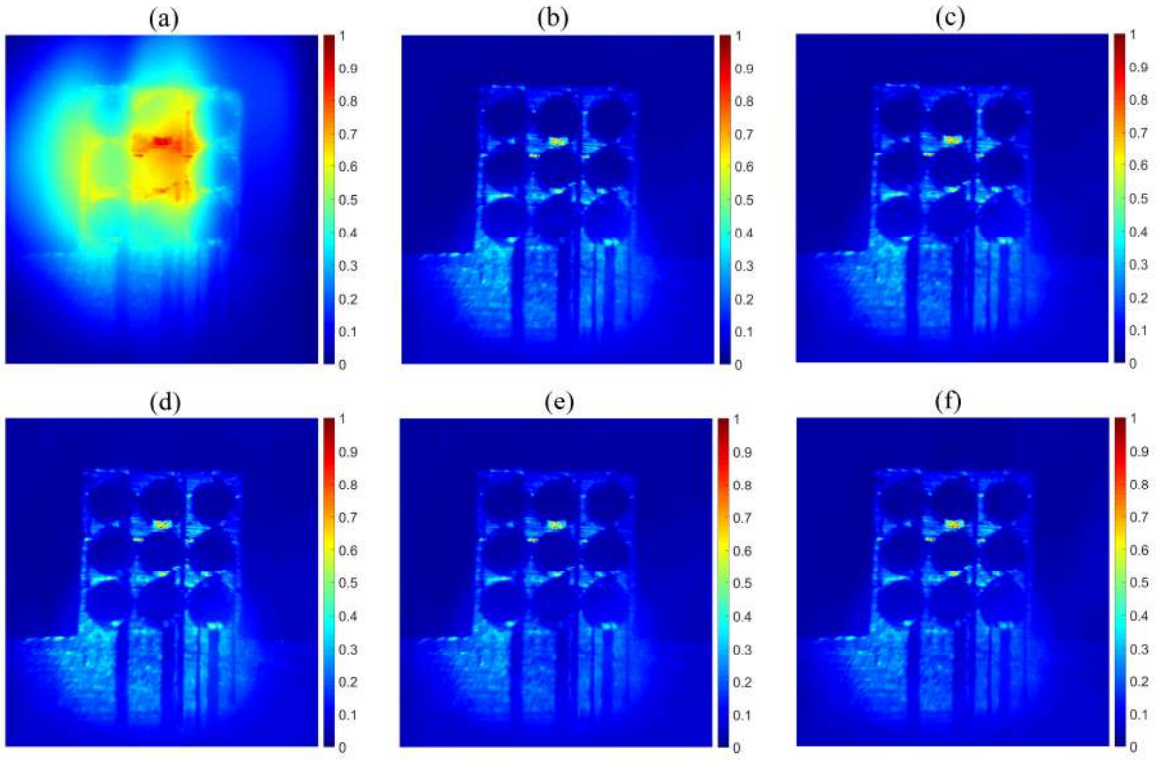

Fig. 4.4. Comparison between the raw image and the processed images for different frame rates with blue light and blue filter. (a) One of the raw images. (b-f) Processed images for frame rates 26, 39, 52, 78, and 104 Hz, respectively.

The image quality of the object is observed to be dependent on the camera settings. We carried out systematic imaging at different frame rates keeping the exposure time (5 ms) and the total number of frames (312) constant. One of the raw frames for frame rate 26 is shown in

Fig. 4.4(a). The processed images shown in Fig. 4.4(b-f) are captured at frame rates of 26, 39, 52, 78, and 104 Hz, respectively. Though we observe a drastic improvement in the processed images, no perceivable changes is observed in the contrast for different frame rates.

Imaging with both flame and smoke

We now discuss our measurements when both flame (using a single candle) and smoke (created in a chamber) are present during the imaging of the object. The effect of smoke is quantified in terms of an attenuation coefficient, which is defined as,

$$\alpha = \frac{1}{l} \ln \frac{I_0}{I} = \frac{1}{l} \ln \frac{V_0}{V} \tag{4.1}$$

where V_0 and V are voltage readings on the oscilloscope corresponding to intensities without and with smoke (I_0 and I respectively), and l is the thickness of the medium.

The object is imaged for different exposure times (in the range of 1 ms to 5 ms) and attenuation coefficients α of the smoke (in the range of 0 to 10.0 m^{-1}), keeping the frame rate (91) and total number of frames (910) constant. Fig. 4.5(a) shows one of the raw images at an exposure time of 1 ms. Fig. 4.5(b-d) show processed images for exposure times of 1 ms, 3 ms, and 5 ms, respectively, and the corresponding α values are 8.6 m^{-1}, 9.1 m^{-1}, and 10.0 m^{-1}, respectively. The object is clearly visible in the processed image despite the presence of flame (from single candle) and smoke. With an increase in the attenuation coefficient, the image appears to be clearer for a higher exposure time.

We quantified the improvement (enhancement) in image visibility resulting from the application of the QLD technique in terms of the contrast ratio (C), defined as the ratio of the contrast of the processed ($C_{processed}$) image to that of the raw (C_{raw}) image. To define the contrast of an image, we have used the Michelson contrast [53]. The most and least intense regions are of the size 10 $\times$ 10 pixels, as shown in Fig. 4.5(a,b). Mathematically,

$$C = \frac{C_{processed}}{C_{raw}} \tag{4.2}$$

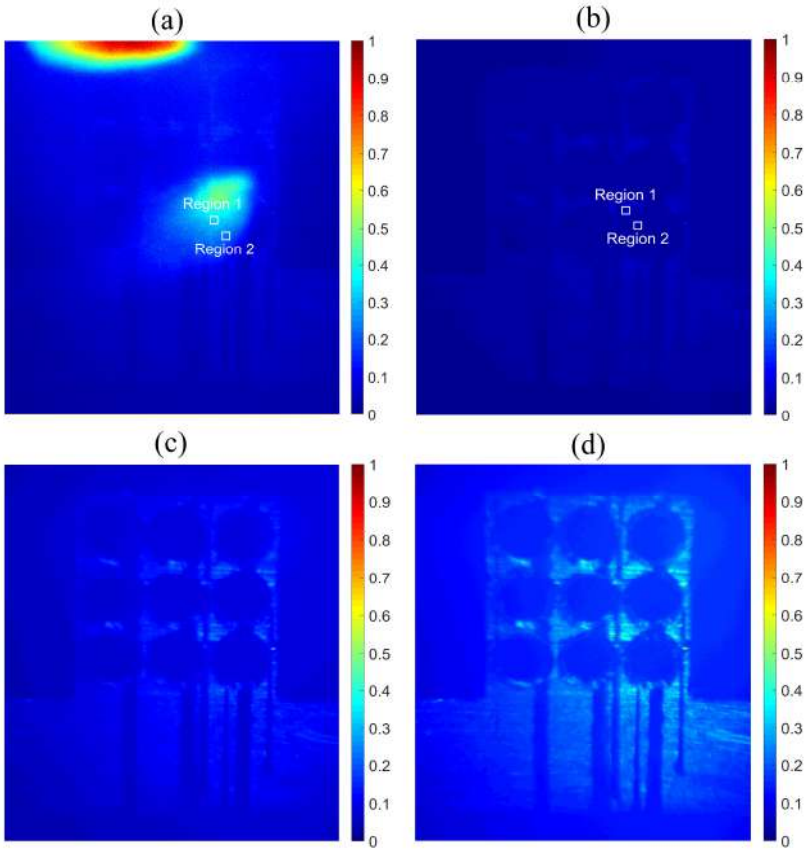

Fig. 4.5. Comparison between the raw image and processed images for different exposure times with blue light and blue filter combination in the presence of both flame and smoke. (a) Saturated raw image of the object. (b-d) Processed images for exposure times of 1 ms, 3 ms, and 5 ms, respectively, and the corresponding α values are 8.6 m^{-1},9.1 m^{-1}, and 10.0 m^{-1}, respectively. The regions marked 1 and 2 are used in estimating the contrast.

and, by definition,

$$C_{raw(processed)} = \frac{\eta_1 - \eta_2}{\eta_1 + \eta_2} \tag{4.3}$$

where, η_1 and η_2 are the average numerical values of all the pixels of the most (region 1) and least (region 2) intense part of the raw (processed) image, respectively, as shown in Fig. 4.5(a,b).

In Fig. 4.6, we compare the contrast ratios of the processed images for different exposure times and attenuation coefficients with blue light and blue filter combination. The enhancement in the contrast of the processed images is nearly 5 times. We observe that when the

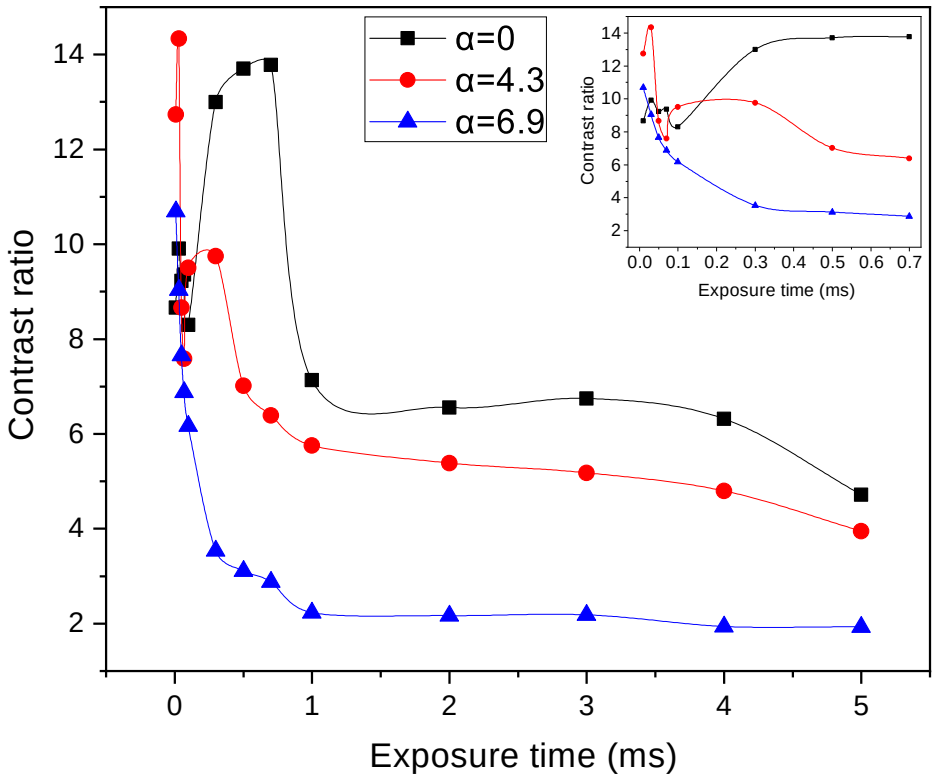

Fig. 4.6. Comparison of the contrast ratios of the processed images for different exposure times and attenuation coefficients with blue light and blue filter combination. Inset shows the expanded view of the graph for exposure time up to 0.7 ms.

exposure times are shorter than 1ms, the contrast ratio is much higher for different attenuation coefficients, although the contrast of the processed image itself is worse than the processed image with the higher exposure time. In addition, the contrast ratio is highest for α =0, i.e., without the smoke, and decreases with an increase in the attenuation coefficient.

As discussed earlier (Fig. 4.3(a,b)), it is evident that, even though the blue filter reduces the intensity of flame emission, the object is not clearly visible even in the absence of smoke. The modulated blue LED light reflected from the object serves as ballistic photons and becomes weaker in the presence of smoke. In the presence of flame and smoke, each pixel of the camera receives blue photons from flame and smoke (diffused photons), and a very small number of blue light photons, reflected from the object (ballistic photons). The observed improvement in the image contrast is because of the operation of the QLD algorithm on the raw image data.

Initially, a copy of the image is made, the first image is multiplied by the reference sinusoid, and the other by a sinusoid 90° phase shifted to the reference. We then obtain components at the modulation frequency, allowing better discrimination of ballistic photons. It has been shown in the case of fog that post-processing of the image, the QLD technique offers a higher contrast-to-noise ratio compared to fast Fourier transform (FFT) [18].

4.4.3 Imaging experiment with white light and blue filter combination

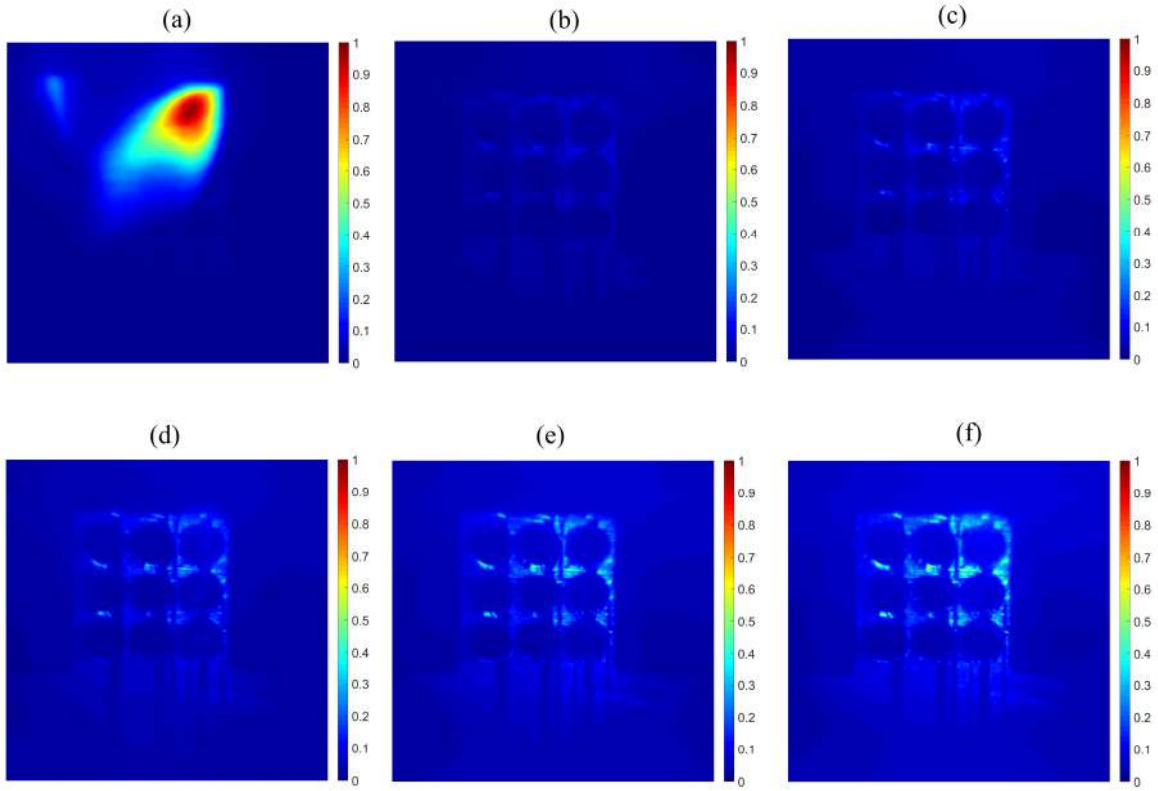

Fig. 4.7. Comparison between the raw image and processed images for different exposure times with white light and blue filter in the presence of flame. (a) Raw image. (b-f) Processed images for exposure times 1 ms, 2 ms, 3 ms, 4 ms, and 5 ms, respectively

In continuation of the above measurements, which used a narrow band light source, we explored the feasibility of our technique with a broadband white LED source as well. We performed imaging of the object in the presence of a single candle flame using white LED and a blue filter. The images are captured keeping the exposure time in the range of 1 ms

to 5 ms. One of the raw images taken for 1 ms exposure time is shown in Fig. 4.7(a). The images, processed by the QLD algorithm, with the frame rate (91) and total number of frames (910) kept constant, are shown in Fig. 4.7(b-f), respectively. The white LED based modulated source also shows a sharp improvement in the contrast that increases with an increase in the exposure time.

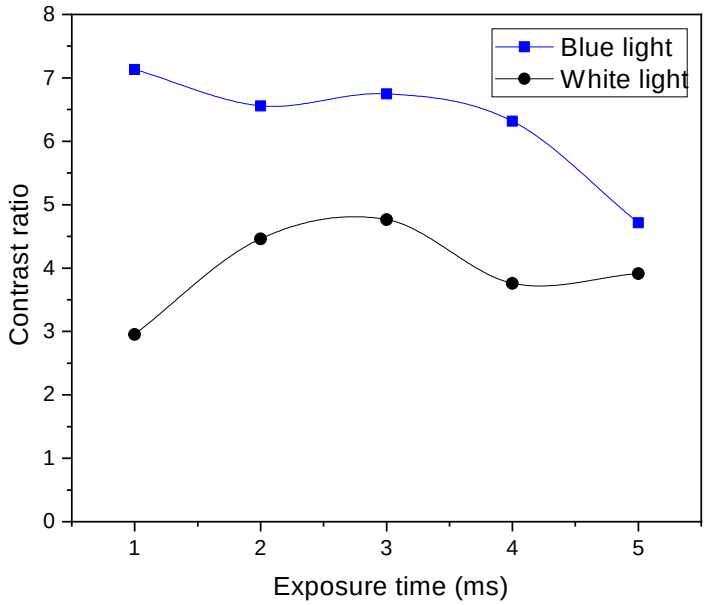

Fig. 4.8. Comparison of contrast ratios obtained for blue LED and white LED with a blue filter in the presence of flame.

When the blue LED is replaced with a white LED, only a narrow blue band transmits through the blue filter, and the red and green portions of the spectrum are blocked. Hence, the net blue power is less when white LED is used (only 3%) as compared to that from a blue LED (21%). The consequence is evident from Fig. 4.8, where the contrast ratio for the blue light and blue filter combination is much higher than for the white light and blue filter combination.

4.4.4 Imaging experiment with red light and red filter combination

However, when we replace the blue LED source and blue filter combination with a red LED and red filter (RG 640), due to increased spectral response of the sCMOS camera around red light and higher intensity of flame transmitted by the red filter, the camera pixels

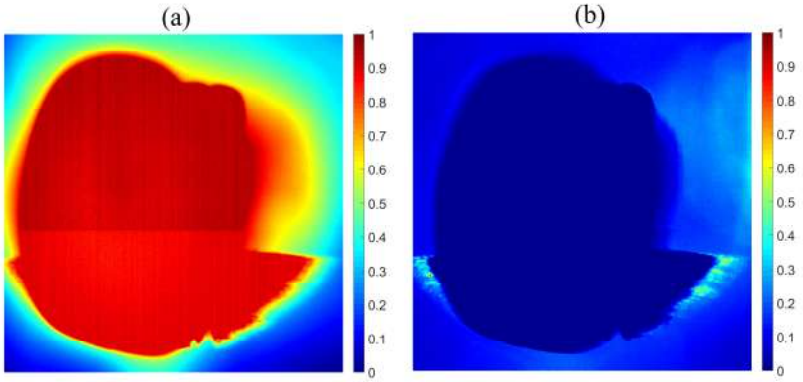

Fig. 4.9. Comparison between the raw and processed image for the red LED and red filter combination in the presence of flame.

are saturated. The saturated raw image and the processed image are shown in Fig. 4.9(a,b). Neither any improvement is observed in the contrast, nor is the object visible after processing the raw images with the QLD algorithm. The exposure time is set at a value of 5 ms.

4.5 Summary

The imaging of an object through fire and smoke in the optical region is a difficult task due to the saturation of the detectors and attenuation of light by scattering and absorption. To the best of our knowledge, this is the first time imaging through both fire and smoke has been performed using the QLD technique. The method uses an incoherent, modulated blue or white light source, along with a blue filter, to image an object through fire and smoke. A candle flame and smoke chamber are used to simulate real-life conditions in the lab. We show that the QLD technique significantly improves the image quality by demonstrating nearly one order of magnitude increase in the contrast ratio. We have also systematically varied the camera parameters such as the exposure time, frame rate, and total number of frames to investigate its effect on the improvement of the image contrast. We then introduce a smoke chamber to simulate a real condition and observe a significant improvement in the image contrast for different exposure times and attenuation coefficients. Although a white LED light source can be used in our technique, blue LED light is preferred because of the higher power

it provides in the narrow blue band. We believe that our technique will be advantageous for improved real-time imaging during firefighting operations. Moreover, the method is simple and cost-effective because it uses an incoherent LED light source, and the QLD algorithm can be easily processed on a personal computer or laptop.

Chapter 5

Imaging using an acousto-optic modulator

Reduced visibility is a common problem when light traverses through a scattering medium, and it becomes difficult to identify an object in such scenarios. A novel proof-of-principle technique for improving image visibility based on the quadrature lock-in discrimination (QLD) algorithm in which the demodulation is performed using an acousto-optic modulator (AOM) is presented here. A significant improvement in image visibility is achieved using a series of frames. We have also performed systematic imaging by varying the camera parameters, such as exposure time, frame rate, and series length, to investigate their effect on enhancing image visibility.

5.1 Introduction

Imaging of an object through a scattering medium, e.g., fog, haze, smoke, etc., has a wide range of potential applications in areas such as medical imaging and navigation, among several others. Imaging through a scattering medium is a challenging task because of the reduced visibility, and in some cases, it becomes impossible to observe the object through the turbid medium. Multiple random scattering from the scatterers strongly degrades the image-bearing capabilities of light and, especially, could bring safety hazards in navigation, like rail and road transport, maritime travel, and aircraft takeoff and landing. Currently, there is no option

other than radio-frequency imaging to overcome this visibility barrier. For objects which emit in the infrared, e.g., human beings, infrared imaging techniques can be used to detect the object. Nevertheless, there is a need for developing imaging techniques that are simple and straightforward in the visible spectral region.

Although extensive research has been conducted in the area of imaging over the last decade [40, 48, 54], imaging through any turbid medium still remains a challenge. One type of 'dehazing' algorithm performs computation techniques using a neural network to make a still-frame clearer, but these techniques still are computationally expensive and complex (e.g., [14]). Another approach utilizes the physical properties of scattering and discriminates between photons taking different types of flight paths. Photons traveling through a scattering medium are generally classified as (i) ballistic photons [1], which are forward scattered and retain the properties such as the direction of propagation, polarization, and phase, (ii) snake photons, which are near forward scattered, and whose path is not far from ballistic photons, and (iii) diffusive photons, that are multiply scattered in random angles over all directions, such that the paths are scrambled, and the original direction is lost. Imaging techniques that exploit a vast amount of diffusive photons use the memory effect and utilize iterative operation like the Richardson-Lucy deconvolution algorithm [6, 7] to restore the undegraded image, but these techniques are time-consuming and mostly need a priori information of the medium [8]. Alternatively, the imaging can be done by extracting the minute amount of ballistic and snake photons from the exceedingly large amount of diffusive photons. This discrimination can be performed by time-gated detection or time-gated holography [3, 21]. However, there exists a simpler, straightforward, and sophisticated approach consisting of a sinusoidally intensity-modulated continuous-wave light source that relies on the characteristic properties of the ballistic photons, which multiply-scattered diffusive photons do not have. This technique requires demodulation of the detected signal at the modulation frequency [17]. This demodulation technique has been demonstrated for a tabletop experiment to image an object through a turbid medium based on the quadrature lock-in discrimination (QLD) algorithm [18], and the technique has been extended to cover a distance of 150 m for imaging

through fog [49]. QLD algorithm has also been performed to image through a flame-and-smoke medium [55]. However, in these scenarios, the signal is recorded in discrete frames, and then multiplication by the sinusoids also happens in a discrete manner. In comparison, the present study proposes a proof-of-principle experiment using an acousto-optic modulator (AOM) to perform the imaging by implementing the multiplication in a continuous mode.

5.2 Principle of QLD technique

The QLD technique explained in Chapter 2 needs to be modified to apply for this case, as the two quadratures as in Eqs. (2.3) and (2.4), will have a DC term, since now the reference sinusoids have an offset. The detailed theory is as follows.

For a light source (such as an LED) that is modulated sinusoidally, the intensity of light can be written as,

$$S = A + B\sin(\omega t + \phi_0) \tag{5.1}$$

where A and B are the offset and amplitude, respectively, ω is the angular frequency, and ϕ_0 is the phase of the modulation. After passing through the turbid medium, the ballistic photons retain the properties such as modulation frequency and phase, with a reduction in intensity. The intensity of the ballistic photons is given by,

$$s = a + b\sin(\omega t + \phi) \tag{5.2}$$

where a and b are the reduced offset and amplitude, respectively, and ϕ is the new phase of the modulation at the detector. Note that although ballistic photons retain the phase, one might start detecting it at a different time, introducing a phase difference.

Now, in the case of using an AOM for demodulation, the multiplication by a sinusoid is implemented by varying the modulation voltage of the AOM driver, which will change the transmissivity of the first order. Since the transmissivity cannot be negative, we need

to multiply the signal by a reference sinusoid with an offset, e.g., $u + v\sin\omega t$ $(u > v)$. So, multiplying Eq. (5.2) by $u + v\sin\omega t$ and $u + v\cos\omega t$, respectively, and integrating over a few cycles (from 0 to NT, where N is the number of cycles and T is the time period of the modulation, i.e., $T = 2\pi/\omega$), we will get

$$q_1 = auNT + \frac{1}{2}bvNT\cos\phi \tag{5.3}$$

and

$$q_2 = auNT + \frac{1}{2}bvNT\sin\phi \tag{5.4}$$

where q_1 and q_2 are known as in-phase and quadrature components.

To find out the values of a, b, and ϕ, we need one more equation, as we have three unknown parameters, i.e., a, b, and ϕ, and two equations. We can see a constant term originating because of the dc component in the reference sinusoids. If we take a dc signal, i.e., u, and multiply it with the signal (Eq. (5.2)), and then integrate, we will get,

$$q_3 = auNT \tag{5.5}$$

Now, if we subtract q_3 from q_1 and q_2, we will only get the sine and cosine terms, and from them, b can be written as,

$$b = \frac{2}{vNT}\sqrt{(q_1 - q_3)^2 + (q_2 - q_3)^2}. \tag{5.6}$$

This is the amplitude of the ballistic modulation. By plotting these values for all the pixels, the image is obtained. The implementation of the QLD technique using Eqs. (5.1) to (5.6) in the form of a block diagram is shown in Fig. 5.1.

Since a camera captures the data in discrete frames, the integrations in Eqs. (5.3) to (5.5) are replaced by summations so that

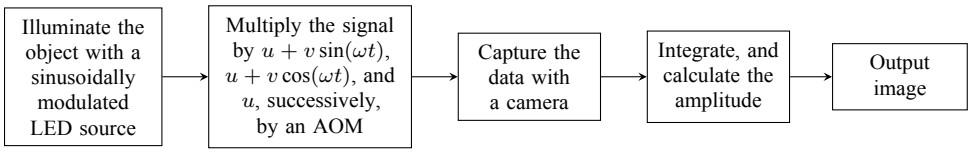

Fig. 5.1. Block diagram of QLD technique.

$$q_{1,2,3} = \sum_i f_i^{(1,2,3)} \tag{5.7}$$

where, f_i's are the discrete frames, and (1,2,3) represent the three quadratures. By using Eqs. (5.6) and (5.7), the value of b is calculated. These numerical values are plotted to obtain a noise-eliminated image of a source in all measurements. The exact code of the simulation is given in Appendix D.

5.3 Experimental setup

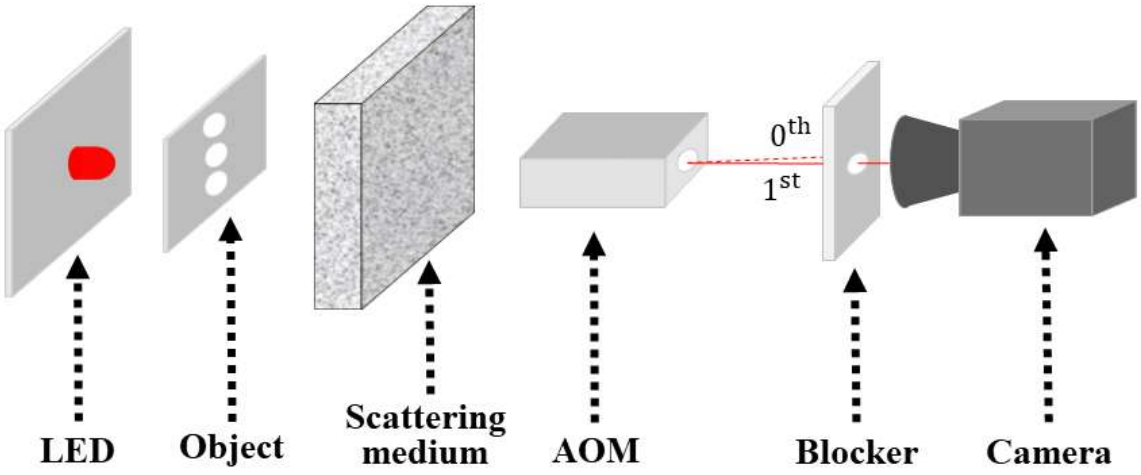

Fig. 5.2. Schematic of the experimental setup. Light from the red LED illuminates the object, and the shadow image falls on the scattering medium. A lens (not in the picture) is used to focus the light onto the AOM, and using a blocker, only the first order is collected by the camera.

Fig. 5.2 shows the schematic of our experimental setup. The object is a rectangular frame sized 5 mm $\times$ 5 mm with three holes that are each 1 mm in diameter and are spaced 1.5 mm apart. We used diluted milk solution as the scattering medium. The attenuation coefficient

of the medium is 2.5 cm^{-1}. As the light source, a 1W red LED (625 nm) is used. To achieve sinusoidal intensity variations, the current passing through the LED is modulated at the frequency of 10 Hz. This modulated light passes through the object and the turbid medium. The scattered light is made to pass through the AOM (ISOMET 1206C), and using a stopper, only the first order light is passed. A lens having 20 cm focal length is used to focus the light onto the AOM crystal. The scattered light is multiplied by sine, cosine, and dc signal, respectively, in the AOM and then gets captured by the camera (16-bit Andor Neo 5.5 sCMOS camera, controlled by Andor Solis software). The AOM is operated at 110 MHz for maximum efficiency. An 8-48 mm F/1–1.2 zoom lens from Ernitec is placed in front of the camera.

We operated the LED, AOM, and camera using a Data Acquisition (DAQ) card (NI 6259) controlled by a LabVIEW program. A continuous signal is generated for LED, and for the AOM, a concatenated signal of sine, cosine, and dc, each having the same time duration and having the same frequency as LED modulation, is generated. The camera, along with the LED and AOM signal voltage, is also triggered at the same time and runs till all the data in a series is captured.

A series of frames are captured at different frame rates (80, 100, 160, 200, 320 Hz) and exposure times (0.1 ms to 1 ms) and are processed using the QLD algorithm. The frame resolution is $\sim 90 \times 60$ pixels. The limiting value of exposure time, frame rate, and the series length depends on the frame resolution and, computer and camera memory.

5.4 Results and discussion

5.4.1 Characterizing the first-order transmissivity of the AOM

In Fig. 5.3, a plot of transmissivity in the first order for different input modulation voltages of the AOM is presented. We need a linear response to vary the transmissivity sinusoidally by varying the input voltage, and the best fit of the plot to a straight line lies within the 1.5 V to 3.5 V of the modulation voltage.

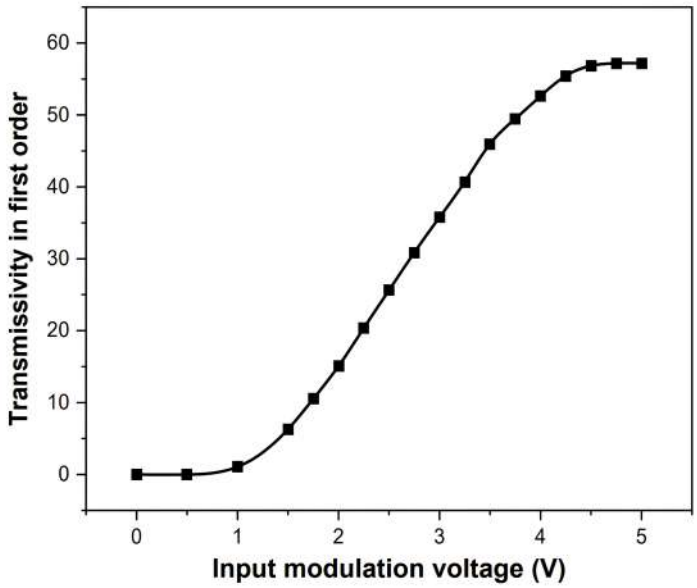

Fig. 5.3. Transmissivity in the first order for different input modulation voltage of the AOM.

5.4.2 Comparison between raw image and processed image

In Fig. 5.4, we show a comparison of (a) a direct raw image in the absence of AOM and (b) the corresponding processed image of the object in the presence of the scattering medium. It is evident from the figure that the QLD algorithm improves visibility by reducing the background noise considerably.

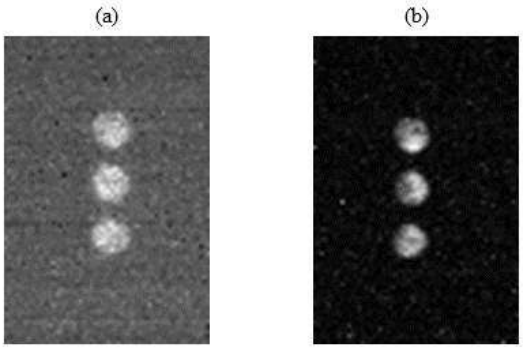

Fig. 5.4. Comparison between a direct raw image of the object and the final processed image. (a) Raw image. (b) Processed image.

5.4.3 Effect of exposure time on the contrast of processed images

It has been observed that the image quality of the object is dependent on the camera settings. We performed systematic imaging for different camera parameters. Exposure time, frame rate, and the series length are varied at a time, while others are kept constant. Fig. 5.5 shows the processed images for different exposure times. By applying the QLD algorithm, keeping the frame rate (80 Hz) and the series length (1600 frames per quadrature signal) constant, we observe a significant improvement in the visibility of the object (Fig. 5.5(a-e)), which increases with increase in the exposure time (for exposure times of 0.1 ms, 0.25 ms, 0.5 ms, 0.75 ms, and 1 ms, respectively).

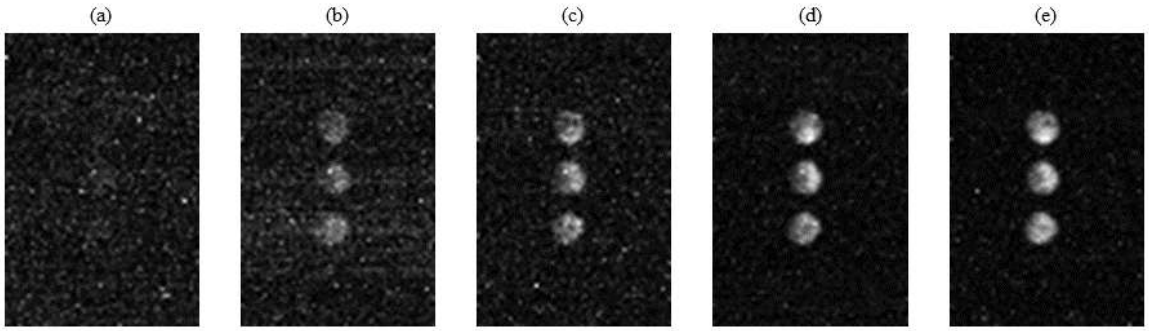

Fig. 5.5. Comparison between the processed images for different exposure times. (a-e) Processed images for exposure times 0.1 ms, 0.25 ms, 0.5 ms, 0.75 ms, and 1 ms, respectively.

5.4.4 Effect of frame rate on the contrast of processed images

We now varied the frame rate, keeping exposure time and the series length constant. The processed images, captured at different frame rates (80 Hz, 100 Hz, 160 Hz, 200 Hz, and 320 Hz, respectively), are shown in Fig. 5.6(a-e). All the processed images are much improved compared to the corresponding raw images, and no perceivable variation is observed in the image visibility for different frame rates.

5.4.5 Effect of series length on the contrast of processed images

The comparison between the processed images for different series lengths is shown in

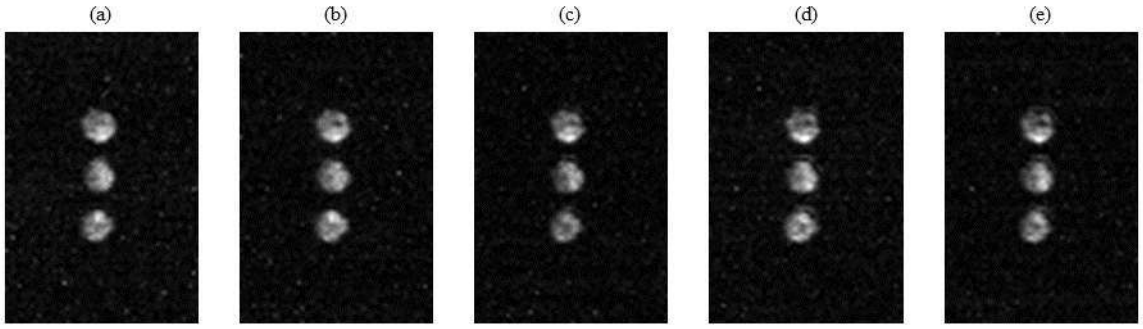

Fig. 5.6. Comparison between the processed images for different frame rates. (a-e) Processed images for frame rates of 80 Hz, 100 Hz, 160 Hz, 200 Hz, and 320 Hz, respectively.

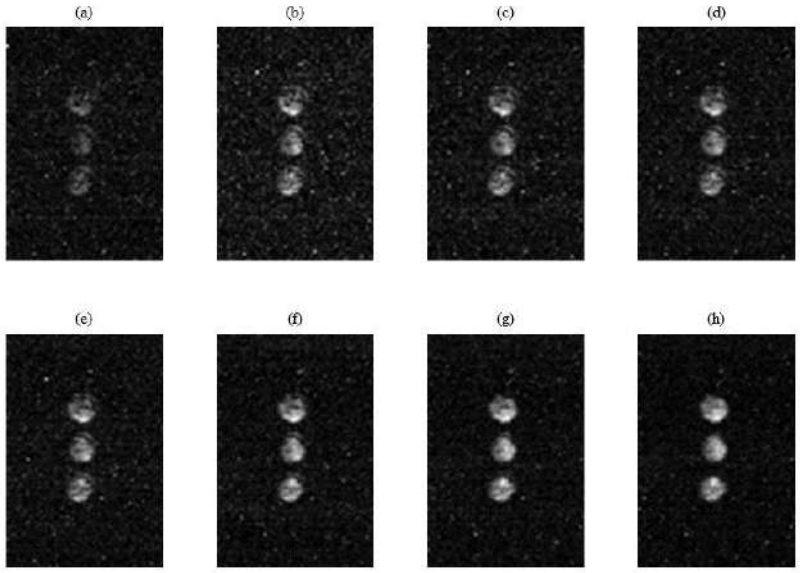

Fig. 5.7. Comparison between the processed images for different series lengths. (a-h) Processed images for series lengths of 80 frames, 160 frames, 240 frames, 320 frames, 400 frames, 800 frames, 1200 frames, and 1600 frames, respectively.

Fig. 5.7. It is evident from the figure that, with the increase in series length, the visibility improves and saturates at $\sim$ 1200 frames.

From the above figures, we can see that the exposure time and the series length affect the imaging quality significantly. Increasing the exposure time increases the signal-to-noise ratio of raw images, which enhances the final image quality, and increasing the series length helps in additional filtering of the noise, thereby further improving the final image quality.

5.5 Summary

The attenuation of light caused by scattering and absorption makes it challenging to image an object through any scattering medium. The method described here uses a modulated, incoherent, continuous light source in conjunction with an AOM to image an object by employing the QLD technique. We have shown that the QLD technique using AOM significantly improves image quality. The dependence of image visibility on camera parameters, such as exposure time, frame rate, and series length, also has been investigated.

Chapter 6

Summary and future prospects

6.1 Summary

In this thesis, imaging through turbid media using a modulated, continuous, incoherent light source and Quadrature Lock-in Discrimination (QLD) technique is studied. The technique is performed on the emerging light from a turbid media.

In **Chapter 1**, a brief introduction to the optical media, turbid media, scattering of light in turbid media, behaviour of photons in these media, and different types of imaging techniques using different types of photons is mentioned.

In **Chapter 2**, the theory of the QLD technique is explained, along with detailed mathematics. The simulation of the same is also explained. The simulation results show a remarkable improvement in the visibility of the processed image compared to the raw images.

In **Chapter 3**, a light source is imaged through fog. The light from the source passes through the scattering medium and is captured by the camera. Along with this, we have tested the application of the QLD technique to an illuminated object that is very close to it. Also, the QLD technique in daylight conditions is tested. In all of the cases, there is a significant improvement in the contrast of the processed image.

In **Chapter 4**, an extension to the previous studies to image an illuminated object by an LED to make the previous study complete is performed. In this case, the medium is flame

and smoke. The light from the LED is made to pass through the medium, reflected by the object, passes through the medium again, and is ultimately captured by the camera.

In **Chapter 5**, what we believe to be a novel proof-of-principle technique to increase image visibility is presented. In this technique, the demodulation is performed using an acousto-optic modulator (AOM). A considerable improvement in image visibility is achieved. Along with this, systematic imaging by varying the camera parameters, such as exposure time, frame rate, and series length, to investigate their effect on enhancing image visibility is also performed.

6.2 Future prospects

This thesis contributes to the imaging through scattering media topic. It is still very far from being realized in practice, but a small step is taken to make it towards the accomplishment. The following works can be performed in future to make it more implementable in real-life:

- The fog experiment can be performed in different places with different types of fog. It should also be performed with moving objects and moving camera. The object size can also be change to see its effect. The imaging should also be done in both transmission and reflection geometry.

- For the fire experiment, a more detail experiment can be performed. One can use a range of different types of source of fire to check it's effect on the blinding of the detector, and consequently on the image contrast. One can also vary the filter bandwidth and source wavelength to check the same.

- For the imaging experiment using AOM, one can try to change the medium concentration to optimize the camera parameter. One can try to increase the efficiency in the first order of the AOM by appropriately choosing the source wavelength and the AOM. Since, it uses LEDs as a light source, optimization of the optical setup is also needs to done.

Besides these steps, one should make these experiments in real-time so that it immediately visible to the observer in a screen. Also, the entire system, i.e., the light source, and the camera (and also the filter for the imaging though flame experiment), should be made in a box so that it can be taken anywhere and installed anywhere. It should be in a size such that it can installed in trains, vehicles, aircraft, submarines, etc. for uninterrupted navigation. Imaging through flame and smoke is beneficial for firefighters. They can simply attach it to their body and perform the search and rescue operation. In this case one can make a goggle in which the view will be shown. It can also be placed in drones to take images from all the side and make a 3D view of the same. Also, in each step, there is an opportunity to enhance the technique. For example, the light sources could be modified to produce more focused light. In our experiments, we utilized a single-photon detector camera (Andor Neo 5.5 sCMOS camera), but a newly developed, more advanced camera with lower noise could yield better signal-to-noise ratio (SNR) and improved image contrast.

Appendix A

The exact code to simulate the QLD technique

A.1 Algorithm

To simulate the technique, we need to understand how a camera would capture a scene with modulated intensity. We could just multiply an image by a sine function to make it modulating, but it would not be exact as intensity can not be negative. To make it non-negative, we could just add 1 to it, but we need to multiply it by 1/2 to change the scale to '0 to 1'. After modulating the image, noise is added. The values are then multiplied by sine and cosine function of the same frequency, respectively. After each multiplication it should be added cumulatively to the sum of the previous terms, which is zero before the first frame. After that, the two terms need to be squared and added, and then the root is to be taken to find the amplitude of the signal. Finally, the scale needs to be changed to '0 to 1' to view it as an image. The modulation-demodulation frequency is 13 Hz for the simulation with a single image. For the simulation with two images, the modulation frequencies are 13 Hz and 17 Hz, and the demodulation frequency can be change to process the QLD technique at different frequencies to get different processed image at different frequency. The sampling frequencies are 260 Hz, and 221 Hz, respectively, for single image simulation and two image simulation,

and the length of the series for both the cases is taken as 13000 frames. Every parameter can be change to optimize its performance. The demodulation frequency can be change to check its feasibility.

A.2 Simulation

A.2.1 Simulation with a single image

```
% import the image and changing the scale to '0 to 1' scale
data=mat2gray(imread('image1.png'));
% extracting the size of the image
sizeOfData=size(data);
% modulation frequency
modulationFrequency=13;
% demodulation frequency
demodulationFrequency=13;
% sampling frequency / frame rate
samplingFrequency=260;
% required number of frames to performed the technique
numberOfFrames=13000;
% allocating the space to store the cumulative summation values after
% the multiplication
% for sine quadrature
sineValue=zeros(sizeOfData);
% for cosine quadrature
cosineValue=zeros(sizeOfData);
% 'for' loop to run through all the frames
for k=1:numberOfFrames
   % modulating the image sinusoidally
   modData=data*1/2*(1+sin(2*pi*k*modulationFrequency
            /samplingFrequency));
   % defining the noise
   noise=10*rand(sizeOfData);
   % adding the noise
   totalNoiseData=modData+noise;
```

```
   % multipling the noisy signal by sine
   sineData=totalNoiseData*sin(2*pi*k*demodulationFrequency
            /samplingFrequency));
   % adding the sine value cumulatively
   sineValue=sineValue+sineData;
   % multipling the noisy signal by cosine
   cosineData=totalNoiseData*cos(2*pi*k*demodulationFrequency
            /samplingFrequency));
   % adding the cosine value cumulatively
   cosineValue=cosineValue+cosineData;
end
% squaring and adding the two quadratures
calData=sineValue.^2+cosineValue.^2;
% taking the square root
sqrtCalData=sqrt(calData);
% changing the scale of the image to '0 to 1' scale
amplitude=mat2gray(sqrtCalData);
% showing the final image
imshow(amplitude)
```

A.2.2 Simulation with two images

```
% import the images and changing the scale to '0 to 1'
% image1
data1=mat2gray(imread('image1.png'));
% image2
data2=mat2gray(imread('image2.png'));
% extracting the size of the image1
% the size of image1 and image2 are already made same
sizeOfData=size(data1);
% modulation frequencies
% modulation frequency1
modulationFrequency1=13;
% modulation frequency2
modulationFrequency2=17;
% demodulation frequency
```

```
demodulationFrequency=13;
% sampling frequency
samplingFrequency=221;
% required number of frames to performed the technique
numberOfFrames=13000;
% allocating the space to store the cumulative summation values after
% the multiplication
% for sine quadrature
sineValue=zeros(sizeOfData);
% for cosine quadrature
cosineValue=zeros(sizeOfData);
% 'for' loop to run through all the frames
for k=1:numberOfFrames
   % modulating the image1 sinusoidally
   modData1=data1*1/2*(1+sin(2*pi*k*modulationFrequency1
            /samplingFrequency));
   % modulating the image2 sinusoidally
   modData2=data2*1/2*(1+sin(2*pi*k*modulationFrequency2
            /samplingFrequency));
   % defining the noise
   noise=10*rand(sizeOfData);
   % adding the noise
   totalNoiseData=modData1+modData2+noise;
   % multipling the noisy signal by sine
   sineData=totalNoiseData*sin(2*pi*k*demodulationFrequency
            /samplingFrequency);
   % adding the sine value cumulatively
   sineValue=sineValue+sineData;
   % multipling the noisy signal by cosine
   cosineData=totalNoiseData*cos(2*pi*k*demodulationFrequency
            /samplingFrequency);
   % adding the cosine value cumulatively
   cosineValue=cosineValue+cosineData;
end
% squaring and adding the two quadratures
calData=sineValue.^2+cosineValue.^2;
```

```
% taking the square root
sqrtCalData=sqrt(calData);
% changing the scale of the image to '0 to 1' scale
amplitude=mat2gray(sqrtCalData);
% showing the final image
imshow(amplitude)
```

Appendix B

The exact code to run the QLD technique for the fog experiment

B.1 Details about the camera, data acquisition, and algorithm

The camera that were used in all the experiment is an sCMOS camera. The name of the model is Andor Neo 5.5. The type of the sensor is front illuminated scientific CMOS. The sensor size is 16.6 mm × 14.0 mm (21.8 mm diagonal) and the pixel size is 6.5 μm × 6.5 μm. The number of active pixels this camera has is 2560 × 2160, approximately 5.5 Megapixel, hence the name '5.5'. The maximum achievable quantum efficiency is 60% at 600 nm. Although, it has both 12 bit and 16 bit data range, we used 16 bit depth in every scenario. Therefore, the value of each pixel can vary between from 0 to 65535. It has two constant pixel readout rate: 200 MHz and 560 MHz. We used the 560 MHz readout rate to increase the frame rate. The camera can be cooled to lower the noise. It is cooled using thermoelectric cooling technology. The minimum temperature that can be achieved in this camera is -40 °C. In the camera there are two shutter modes: Rolling and Global (Snapshot) shutter. Since, we needed to capture the whole scene at once, we used global shutter. The typical pixel well

depth is 30000 e^-, and the RMS readout noise for our setting (560 MHz readout rate, global shutter) is 2.8 e^-. Hence, the actual bit depth of the camera is 13.4, obtained from the ratio of the pixel well depth to the RMS read noise. Therefore, the ADC circuit is made to change the bit depth from 13.4 to 16 or 12 depending on the data range instruction. The camera is connected to the computer using a Camera Link connector cable to the PCIe slot in the computer. The computer used for this is a Dell Tower computer with 64 GB RAM, 1 TB ROM, and a 4 GB Nvidia graphics card. The camera can be controlled by the Andor Solis software to give the input of different parameters, and to save the data. It can also be accessed by different programming languages using the API. In the Solis software, immediately after capturing the data is shown as an image. The data can also be saved (exported) as different format, e.g., sif, tif/tiff, jpg, png, avi, mpeg, ascii, dat, etc. To only view the data the best file type is jpg, but to do the calculation on the pixel values, dat file is best, since it takes less amount of storage. It saves the 16 bit binary data as 2 bytes information separately in decimal values one after another with no space between them. Also, each pixel value are placed one after another with no space either. There is also no space in between the images. Therefore, a small algorithm needs to be applied to change it to proper decimal values. To find the value of the pixel, the left byte value is multiplied by 256, since it is 8 bit above the right byte value, and then the right byte value should be added. To store the pixel data, 1D arrays are created, since it is easier to handle than 2D image. The flattened raw data of the frames is read one by one, and then converted to pixel value. After changing the values of all the pixels to decimal values, we will apply the demodulation part of the QLD technique, i.e., multiplying by sine and cosine function, respectively, and then summing up the data. As in the simulation, we calculate the square of the two quadratures, and then take the square root of the sum of the said two square terms. Since, the data still is in an 1D array format, it needs to be reshaped to an image. To show the data as an image, the scale of the image needs to changed to ‘0 to 1’ scale. Lastly, the pixels values needs to be shown as image. The output can also be exported as jpg, png, tif, dat, etc.

B.2 Code

```
% import the data and changing the scale of the image to '0 to 1'
fileId=fopen('fileName.dat');
% mentioning the size of the images
% width
width=70;
% height
height=50;
% calculating the total number of pixels in an image
numberOfPixels=height*width;
% demodulation frequency
demodulationFrequency=13;
% sampling frequency / frame rate
frameRate=260;
% required number of frames to performed the technique
numberOfFrames=10140;
% allocating the space to store the cumulative summation values after
% the multiplication
% for sine quadrature
sineValue=zeros(1,numberOfPixels);
% for cosine quadrature
cosineValue=zeros(1,numberOfPixels);
% 'for' loop to run through all the frames
for m=1:numberOfFrames
   % reading the image data which is equal to twice the number
   % of pixels as there is 2 bytes per pixel
   dataLine=fread(fileId,2*numberOfPixels);
   % allocating the space to store each pixels value
   dataM=zeros(1,numberOfPixels);
   % 'for' loop to run through all the pixels to calculate
   % its proper value in decimal
   for k=1:numberOfPixels
      % calculating the value of the pixel and storing it
      % in the element
      dataM(k)=dataLine(2*k)*256+dataLine(2*k-1);
```

```
   end
   % multipling the values by sine
   sineData=dataM*sin(2*pi*m*demodulationFrequency/frameRate));
   % adding the sines value cumulatively
   sineValue=sineValue+sineData;
   % multipling the data by cosine
   cosineData=dataM*cos(2*pi*m*demodulationFrequency/frameRate));
   % adding the cosine value cumulatively
   cosineValue=cosineValue+cosineData;
end
% squaring and adding the two quadratures
calData=sineValue.^2+cosineValue.^2;
% taking the square root
sqrtCalData=sqrt(calData);
% as the data is in a 1D array, its need to be changed to an 2D array
% as in an image
% reshaping the image
reSqrtCalData=reshape(sqrtCalData,width,height);
% inverting the image to make it proper
flipReSqrtCalData=flip(reSqrtCalData');
% changing the scale of the image to '0 to 1' scale
amplitude=mat2gray(flipReSqrtCalData);
% showing the final image
imshow(amplitude)
% closing the file
fclose('fileId');
```

Appendix C

The exact code to run the QLD technique for the fire and smoke experiment

C.1 Algorithm

The algorithm is same as described in Appendix B.

C.2 Code

```
% import the data and changing the scale of the image to '0 to 1'
fileId=fopen('fileName.dat');
% mentioning the size of the images
% width
width=600;
% height
height=600;
% calculating the total number of pixels in an image
numberOfPixels=height*width;
% demodulation frequency
demodulationFrequency=13;
% sampling frequency / frame rate
frameRate=91;
```

```
% required number of frames to performed the technique
numberOfFrames=455;
% allocating the space to store the cumulative summation values after
% the multiplication
% for sine quadrature
sineValue=zeros(1,numberOfPixels);
% for cosine quadrature
cosineValue=zeros(1,numberOfPixels);
% 'for' loop to run through all the frames
for m=1:numberOfFrames
   % reading the image data which is equal to twice the number
   % of pixels as there is 2 bytes per pixel
   dataLine=fread(fileId,2*numberOfPixels);
   % allocating the space to store each pixels value
   dataM=zeros(1,numberOfPixels);
   % 'for' loop to run through all the pixels to calculate
   % its proper value in decimal
   for k=1:numberOfPixels
      % calculating the value of the pixel and storing it
      % in the element
      dataM(k)=dataLine(2*k)*256+dataLine(2*k-1);
   end
   % multipling the values by sine
   sineData=dataM*sin(2*pi*m*demodulationFrequency/frameRate));
   % adding the sines value cumulatively
   sineValue=sineValue+sineData;
   % multipling the data by cosine
   cosineData=dataM*cos(2*pi*m*demodulationFrequency/frameRate));
   % adding the cosine value cumulatively
   cosineValue=cosineValue+cosineData;
end
% squaring and adding the two quadratures
calData=sineValue.^2+cosineValue.^2;
% taking the square root
sqrtCalData=sqrt(calData);
% as the data is in a 1D array, its need to be changed to an 2D array
```

```
% as in an image
% reshaping the image
reSqrtCalData=reshape(sqrtCalData,width,height);
% inverting the image to make it proper
flipReSqrtCalData=flip(reSqrtCalData');
% changing the scale of the image to '0 to 1' scale
amplitude=mat2gray(flipReSqrtCalData);
% showing the final image
imshow(amplitude)
% closing the file
fclose('fileId');
```

Appendix D

The exact code to run the QLD technique for the imaging with AOM experiment

D.1 Algorithm

Since, in this experiment, the multiplication as already applied by the AOM, only the cumulative addition needs to be performed by the code. The sine, cosine, and dc data is collected in serial. Therefore, the calculation will run one after another. First, there will be calculation for sine quadrature, followed by cosine and dc. Then, the dc values is subtracted from the sine and cosine values, and followed by squaring and addition of those two terms.

D.2 Code

```
% import the data and changing the scale of the image to '0 to 1'
fileId=fopen('fileName.dat');
% mentioning the size of the images
% width
width=60;
% height
height=90;
% calculating the total number of pixels in an image
```

```
numberOfPixels=height*width;
% required number of frames to performed the technique
numberOfFrames=1600;

% sine quadrarure calculation
% allocating the space to store the value
sineValue=zeros(1,numberOfPixels);
% 'for' loop to run through all the frames for sine quadrature
for m=1:numberOfFrames
   % reading the image data which is equal to twice the number
   % of pixels as there is 2 bytes per pixel
   dataLine=fread(fileId,2*numberOfPixels);
   % allocating the space to store each pixels value
   dataM=zeros(1,numberOfPixels);
   % 'for' loop to run through all the pixels to calculate
   % its proper value in decimal
   for k=1:numberOfPixels
      % calculating the value of the pixel and storing it
      % in the element
      dataM(k)=dataLine(2*k)*256+dataLine(2*k-1);
   end
   % adding the sines value cumulatively
   sineValue=sineValue+dataM;
end

% cosine quadrarure calculation
% allocating the space to store the value
cosineValue=zeros(1,numberOfPixels);
% 'for' loop to run through all the frames for sine quadrature
for m=1:numberOfFrames
   % reading the image data which is equal to twice the number
   % of pixels as there is 2 bytes per pixel
   dataLine=fread(fileId,2*numberOfPixels);
   % allocating the space to store each pixels value
   dataM=zeros(1,numberOfPixels);
   % 'for' loop to run through all the pixels to calculate
```

```
   % its proper value in decimal
   for k=1:numberOfPixels
      % calculating the value of the pixel and storing it
      % in the element
      dataM(k)=dataLine(2*k)*256+dataLine(2*k-1);
   end
   % adding the sines value cumulatively
   cosineValue=cosineValue+dataM;
end

% dc quadrarure calculation
% allocating the space to store the value
dcValue=zeros(1,numberOfPixels);
% 'for' loop to run through all the frames for sine quadrature
for m=1:numberOfFrames
   % reading the image data which is equal to twice the number
   % of pixels as there is 2 bytes per pixel
   dataLine=fread(fileId,2*numberOfPixels);
   % allocating the space to store each pixels value
   dataM=zeros(1,numberOfPixels);
   % 'for' loop to run through all the pixels to calculate
   % its proper value in decimal
   for k=1:numberOfPixels
      % calculating the value of the pixel and storing it
      % in the element
      dataM(k)=dataLine(2*k)*256+dataLine(2*k-1);
   end
   % adding the sines value cumulatively
   dcValue=dcValue+dataM;
end


% subtracting the dc value from sine and cosine value, respectively
% then squaring and adding the two terms
calData=((sineValue-dcValue).^2+(cosineValue-dcValue).^2);
% taking the square root
sqrtCalData=sqrt(calData);
```

```
% as the data is in a 1D array, its need to be changed to an 2D array
% as in an image
% reshaping the image
reSqrtCalData=reshape(sqrtCalData,width,height);
% inverting the image to make it proper
flipReSqrtCalData=flip(reSqrtCalData');
% changing the scale of the image to '0 to 1' scale
amplitude=mat2gray(flipReSqrtCalData);
% showing the final image
imshow(amplitude)
% closing the file
fclose('fileId');
```

Bibliography

[1] Kyung M. Yoo and Robert R. Alfano, *Time-resolved coherent and incoherent components of forward light scattering in random media*, Optics Letters **15**, 320 (1990).

[2] Yves Bérubé-Lauzière, Matteo Crotti, Simon Boucher, Seyedrohollah Ettehadi, Julien Pichette, and Ivan Rech, *Prospects on Time-Domain Diffuse Optical Tomography Based on Time-Correlated Single Photon Counting for Small Animal Imaging*, Journal of Spectroscopy **2016**, 1 (2016).

[3] Christopher Dunsby and Paul M W French, *Techniques for depth-resolved imaging through turbid media including coherence-gated imaging*, Journal of Physics D: Applied Physics **36**, R207 (2003).

[4] Bidyut B. Das, Kyung M. Yoo, and Robert R. Alfano, *Ultrafast time-gated imaging in thick tissues: a step toward optical mammography*, Optics Letters **18**, 1092 (1993).

[5] Michael S. Patterson, Brian C. Wilson, and Douglas R. Wyman, *The propagation of optical radiation in tissue I. Models of radiation transport and their application*, Lasers in Medical Science **6**, 155 (1991).

[6] William H. Richardson, *Bayesian-Based Iterative Method of Image Restoration*∗, Journal of the Optical Society of America **62**, 55 (1972).

[7] L. B. Lucy, *An iterative technique for the rectification of observed distributions*, The Astronomical Journal **79**, 745 (1974).

[8] Eitan Edrei and Giuliano Scarcelli, *Memory-effect based deconvolution microscopy for super-resolution imaging through scattering media*, Scientific Reports **6**, 33558 (2016).

[9] G. E. Anderson, Feng Liu, and Robert R. Alfano, *Microscope imaging through highly scattering media*, Optics Letters **19**, 981 (1994).

[10] M. Minsky, *Microscopy Apparatus*, USA (1961).

[11] J. G. Fujimoto, C. A. Puliafito, R. Margolis, A. Oseroff, S. De Silvestri, and E. P. Ippen, *Femtosecond optical ranging in biological systems*, Optics Letters **11**, 150 (1986).

[12] Jennifer Watson, Patrick Georges, Thierry Lépine, Bruno Alonzi, and Alain Brun, *Imaging in diffuse media with ultrafast degenerate optical parametric amplification*, Optics Letters **20**, 231 (1995).

[13] David Huang, Eric A. Swanson, Charles P. Lin, Joel S. Schuman, William G. Stinson, Warren Chang, Michael R. Hee, Thomas Flotte, Kenton Gregory, Carmen A. Puliafito, and James G. Fujimoto, *Optical Coherence Tomography*, Science **254**, 1178 (1991).

[14] Md. I. Anwar and Arun Khosla, *Vision enhancement through single image fog removal*, Engineering Science and Technology, an International Journal **20**, 1075 (2017).

[15] Hyeonseung Yu, Jongchan Park, KyeoReh Lee, Jonghee Yoon, KyungDuk Kim, Shin-wha Lee, and YongKeun Park, *Recent advances in wavefront shaping techniques for biomedical applications*, Current Applied Physics **15**, 632–641 (2015).

[16] Richard Burdett, *Amplitude Modulated Signals: The Lock-in Amplifier*, in *Handbook of Measuring System Design*, John Wiley & Sons, Inc. (2005).

[17] Linda Mullen, Alan Laux, Brandon Cochenour, Eleonora P. Zege, Iosif L. Katsev, and Alexander S. Prikhach, *Demodulation techniques for the amplitude modulated laser imager*, Applied Optics **46**, 7374 (2007).

[18] Sriram Sudarsanam, James Mathew, Swapnesh Panigrahi, Julien Fade, Mehdi Alouini, and Hema Ramachandran, *Real-time imaging through strongly scattering media: seeing through turbid media, instantly*, Scientific Reports **6**, 25033 (2016).

[19] Hema Ramachandran, *Imaging through turbid media*, Current Science **76**, 1334 (1999).

[20] Ofer David, Norman S. Kopeika, and Boaz Weizer, *Range gated active night vision system for automobiles*, Applied Optics **45**, 7248 (2006).

[21] Andrei V. Kanaev, Abbie T. Watnik, Dennis F. Gardner, Christopher Metzler, Kyle P. Judd, Paul Lebow, Kimberly M. Novak, and James R. Lindle, *Imaging through extreme scattering in extended dynamic media*, Optics Letters **43**, 3088 (2018).

[22] Guy Satat, Matthew Tancik, and Ramesh Raskar, *Towards photography through realistic fog*, in *IEEE International Conference on Computational Photography (ICCP)*, IEEE (2018).

[23] Sébastien Popoff, Geoffroy Lerosey, Mathias Fink, Albert Claude Boccara, and Sylvain Gigan, *Image transmission through an opaque material*, Nature Communications **1**, 81 (2010).

[24] Ori Katz, Eran Small, and Yaron Silberberg, *Looking around corners and through thin turbid layers in real time with scattered incoherent light*, Nature Photonics **6**, 549 (2012).

[25] Jacopo Bertolotti, Elbert G. van Putten, Christian Blum, Ad Lagendijk, Willem L. Vos, and Allard P. Mosk, *Non-invasive imaging through opaque scattering layers*, Nature **491**, 232 (2012).

[26] Olivier Emile, Fabien Bretenaker, and Albert Le Floch, *Rotating polarization imaging in turbid media*, Optics Letters **21**, 1706 (1996).

[27] Hema Ramachandran and Andal Narayanan, *Two-dimensional imaging through turbid media using a continuous wave light source*, Optics Communications **154**, 255 (1998).

[28] Swapnesh Panigrahi, Julien Fade, Romain Agaisse, Hema Ramachandran, and Mehdi Alouini, *An all-optical technique enables instantaneous single-shot demodulation of images at high frequency*, Nature Communications **11**, 549 (2020).

[29] J. Allen Zak. Drop size distributions and related properties of fog for five locations measured from aircraft. https://ntrs.nasa.gov/citations/19940028559. Accessed: July 15, 2023.

[30] Place of Occurrence-wise Number of Fire Accidents, Persons Injured and Died during 2019 (All India), National Crime Records Bureau, India. https://ncrb.gov.in/sites/default/files/adsi_reports_previous_year/Table-1.10_2019.pdf. Accessed: July 15, 2023.

[31] U. S. Fire Administration. https://www.usfa.fema.gov/data/statistics/. Accessed: July 15, 2023.

[32] Mark Harris, *The way through the flames*, IEEE Spectrum **50**, 30 (2013).

[33] Teledyne FLIR LLC. https://www.flir.com/. Accessed: July 15, 2023.

[34] Jenoptik AG. https://www.flir.com/. Accessed: July 15, 2023.

[35] Paul W. Kruse, *Uncooled Thermal Imaging: Arrays, Systems, and Applications*, SPIE Press (2001).

[36] Joseph S. Accetta, *Sensors, Infrared*, in *Encyclopedia of Applied Physics*, John Wiley & Sons, Inc. (2003).

[37] Bruno Fieque, Patrick Robert, Christophe Minassian, Michel Vilain, Jean L. Tissot, Arnaud Crastes, Olivier Legras, and Jean J. Yon, *Uncooled amorphous silicon XGA IRFPA with 17μm pixel-pitch for high end applications*, in *Proceedings of SPIE*, **6940**, 69401X, Infrared Technology and Applications XXXIV (2008).

[38] Vittorio Bianco, Melania Paturzo, Andrea Finizio, Karl A. Stetson, and Pietro Ferraro, *Portable IR Laser System for Real-Time Display of Alive People in Fire Scenes*, Journal of Display Technology **11**, 834 (2015).

[39] Tatiana Grulois, Guillaume Druart, Nicolas Guérineau, Arnaud Crastes, Hervé Sauer, and Pierre Chavel, *Extra-thin infrared camera for low-cost surveillance applications*, Optics Letters **39**, 3169 (2014).

[40] Massimiliano Locatelli, Eugenio Pugliese, Melania Paturzo, Vittorio Bianco, Andrea Finizio, Anna Pelagotti, Pasquale Poggi, Lisa Miccio, Riccardo Meucci, and Pietro Ferraro, *Imaging live humans through smoke and flames using far-infrared digital holography*, Optics Express **21**, 5379 (2013).

[41] Eric W. Mitchell, Matthew S. Hoehler, Fabrizio R. Giorgetta, Torrey Hayden, Gregory B. Rieker, Nathan R. Newbury, and Esther Baumann, *Coherent laser ranging for precision imaging through flames*, Optica **5**, 988 (2018).

[42] Vittorio Bianco, Pier L. Mazzeo, Melania Paturzo, Cosimo Distante, and Pietro Ferraro, *Deep learning assisted portable IR active imaging sensor spots and identifies live humans through fire*, Optics and Lasers in Engineering **124**, 105818 (2020).

[43] Matthew S. Hoehler and Christopher M. Smith, *Application of blue laser triangulation sensors for displacement measurement through fire*, Measurement Science and Technology **27**, 115201 (2016).

[44] Christopher M. Smith and Matthew S. Hoehler, *Imaging Through Fire Using Narrow-Spectrum Illumination*, Fire Technology **54**, 1705 (2018).

[45] Thomas Spirig, Philipp Seitz, Oliver Vietze, and Friedrich Heitger, *The lock-in CCD-two-dimensional synchronous detection of light*, IEEE Journal of Quantum Electronics **31**, 1705 (1995).

[46] Yoav Y. Schechner, Srinivasa G. Narasimhan, and Shree K. Nayar, *Polarization-based vision through haze*, Applied Optics **42**, 511 (2003).

[47] Fei Liu, Lei Cao, Xiaopeng Shao, Pingli Han, and Xiangli Bin, *Polarimetric dehazing utilizing spatial frequency segregation of images*, Applied Optics **54**, 8116 (2015).

[48] Julien Fade, Swapnesh Panigrahi, Anthony Carré, Ludovic Frein, Cyril Hamel, Fabien Bretenaker, Hema Ramachandran, and Mehdi Alouini, *Long-range polarimetric imaging through fog*, Applied Optics **53**, 3854 (2014).

[49] Shashank Kumar, Bapan Debnath, Meena M. S., Julien Fade, Sankar Dhar, Mehdi Alouini, Fabien Bretenaker, and Hema Ramachandran, *Imaging through fog using quadrature lock-in discrimination*, OSA Continuum **4**, 1649 (2021).

[50] Chi-Ru Yang, Ta-Chang Lin, and Feng-Hsiang Chang, *Particle size distribution and PAH concentrations of incense smoke in a combustion chamber*, Environmental Pollution **145**, 606 (2007).

[51] Siao W. See, Rajasekhar Balasubramanian, and Umid M. Joshi, *Physical characteristics of nanoparticles emitted from incense smoke*, Science and Technology of Advanced Materials **8**, 25 (2007).

[52] Aditya A. Roy, Sanjay P. Baxla, Tarun Gupta, Rajdip Bandyopadhyaya, and Sachchida N. Tripathi, *Particles emitted from indoor combustion sources: size distribution measurement and chemical analysis*, Inhalation Toxicology **21**, 837 (2009).

[53] Albert A. Michelson, *Studies in Optics*, Dover Publications, Inc. (1995).

[54] David B. Lindell and Gordon Wetzstein, *Three-dimensional imaging through scattering media based on confocal diffuse tomography*, Nature Communications **11**, 4517 (2020).

[55] Bapan Debnath, Jayashree A. Dharmadhikari, Meena M. S., Hema Ramachandran, and Aditya K. Dharmadhikari, *Improved imaging through flame and smoke using blue LED*

and quadrature lock-in discrimination algorithm, Optics and Lasers in Engineering **154**, 107045 (2022).